DEVELOPMENT OF A DIRECT-FORCE-READING, THIN-FILM SHEAR STRESS GAGE

by

James M. Putz

Thesis submitted to the Faculty of the

Virginia Polytechnic Institute and State University

in partial fulfillment of the requirements for the degree of

Master of Science

in

Mechanical Engineering

APPROVED:

Thomas E. Diller, Chairman

Alfred L. Wicks

Wing F. Ng

January, 1991

Blacksburg, Virginia

DEVELOPMENT OF A DIRECT-FORCE-READING, THIN-FILM SHEAR STRESS GAGE

by

James M. Putz

Thomas E. Diller, Chairman

Mechanical Engineering

(ABSTRACT)

A thin-film gage was designed, constructed, and tested for the measurement of skin friction in steady and non-steady flows. This direct-force-reading gage is designed to have a high frequency response (> 1 kHz), high temperature capability (800 K), and full directional sensitivity in both subsonic and supersonic flows. The thin-film gage consists of a floating element attached to the wall surface by four tabs. The floating element consists of a thin metal film mounted flush to the wall surface. Shear forces acting on the thin-film surface cause strain concentrations to develop in the attachment tabs where strain sensors are located. The shear forces are related to the differential output of the strain sensors located on each of the orthogonal axes of the thin-film gage. A large-scale (10X) prototype was constructed and statically calibrated for actual shear stress measurements. Subsonic, steady flow tests demonstrated the directional sensitivity capability and gave reasonable shear measurements compared to Preston tube results. Subsonic, non-steady flow tests demonstrated the high frequency response of the thin-film gage. Supersonic flow testing was performed which identified design flaws in the original design which were corrected in the development of an actual-size (1X) prototype. Survival of the thin-film gage in a supersonic environment was demonstrated with the 1X prototype. Finally, the 1X prototype was statically calibrated for measurements of shear stress in a supersonic environment.

Acknowledgements

The author would like to give sincere thanks to his advisor, Dr. Tom E. Diller, for the opportunity and assistance provided for this research. The author also extends thanks to Dr. W. F. Ng and Dr. A. L. Wicks for serving on his advisory committee and for their invaluable advice, and the Aeronautical and Ocean Engineering Department of Virginia Tech for the use of their wind tunnel facilities.

The author would also like to thank the United States Air Force, the Marquardt Corporation, and NASA - Langley Research Center for providing funding for this research.

Finally, the author would like to thank his parents for their support which made the author's education possible.

Table of Contents

List of Illustrations

List of Tables

Nomenclature

A,B	hot-wire power/shear stress relationship constants
A_c	strain tab cross-sectional area
A_{gage}	thin-film surface area
c	lip size of floating element used in Allen [30,31]
c	damping coefficient
c_{cr}	critical damping coefficient
C_f	skin friction coefficient
d	Pitot tube diameter
D	head size of floating element used in Allen [30,31]
e	power supplied to hot-wire element
E	modulus of elasticity
E_{in}	input voltage to Wheatstone bridge
E_{out}	output voltage of Wheatstone bridge
f_n	natural frequency (Hz)
F	force acting on thin-film
F_s	shear force

g	gap size of floating element used in Allen [30,31]
G	amplifier gain
GF	gage factor
k	stiffness of strain tab
k_f	fluid thermal conductivity
L	length of strain tab
m	mass of thin-film
M	Mach number
p	pressure
P_p	pitot tube pressure
q	flow trajectory
q″	wall heat flux
R	resistance
Re	Reynold's number
T	temperature
T_{gage}	thin-film temperature
T_{wall}	wall surface temperature
u	local flow velocity
u^*	friction velocity
x, y	coordinate system position
X	displacement of thin-film

greek letters

δ_f	fluid layer thickness
ε	strain
ζ	damping ratio

Θ	momentum thickness
μ_f	absolute viscosity of fluid
ν	kinematic viscosity of fluid
π	3.1415927...
ρ	density of fluid
τ_w	wall shear stress
ϕ	phase angle
ω	frequency (rad/sec)
ω_n	natural frequncy (rad/sec)

Chapter 1

INTRODUCTION

RATIONALE FOR THE RESEARCH

The accurate measurement of wall shear stress (skin friction) is necessary for both theoretically characterizing turbulent boundary layer flow, and for the practical evaluation of aerodynamic performance. In addition to obtaining estimates of skin friction in steady flows, the time-resolved measurement of skin friction in unsteady flows is necessary to improve the understanding of fluid turbulence. The mean shear stress determines the overall frictional drag on an object, while transient fluctuations in shear stress give information about transition, momentum transfer to the wall, and other fluid phenomena. Recently there has been interest in gaining a physical understanding of large-scale fluid structure through time-resolved measurements of local fluid characteristics.

The experimental measurement of skin friction provides information from which empirical relations are formed to characterize turbulent boundary layer flows. Turbu-

lence modelling correlations are based upon the "friction velocity", u^*, for scaling the boundary layer velocity profiles. This quantity, defined by,

$$u^* = \left(\frac{\tau_w}{\rho} \right)^{1/2} \qquad [1.1]$$

depends on accurate estimations of skin friction. Practical measurements of skin friction are needed for accurate predictions of frictional drag on aerodynamic bodies. More specifically, skin friction is a critical factor in supersonic combustion ramjet (SCRAMJET) combustor performance. The available thrust from the engine is greatly reduced by the skin friction in the combustor chamber, making this an important quantity to accurately measure.

OBJECTIVE OF THE RESEARCH

Reliable skin friction measurements in a scramjet combustor are difficult to obtain because of the severe temperature, heat flux, and velocity environments. Current direct measuring devices, i. e., floating element balance, do not achieve the necessary frequency response to make detailed time-resolved measurements of transient fluctuations in skin friction. The thin-film shear stress gage is a new technique of measuring skin friction which could overcome the limitations associated with these current devices such as temperature differences between the wall and sensing elements, unit size, and effects of accelerations. This direct-force-reading gage is designed to have high temperature capability, high frequency response for non-steady measurements, and full directional sensitivity. The latter of these qualities is important for three-dimensional and reversing

flows present in many flow situations. These capabilities would provide a significant advancement to existing skin-friction measurement technology. After reviewing existing measurement methods, the thin-film gage development consisted of the design, fabrication, and bench testing of the thin-film concept for the eventual use in actual scramjet testing.

SCOPE OF THE RESEARCH

The first phase in the development of the thin-film skin-friction gage was to develop a working prototype of the thin-film concept. A ten-times scale (10X) prototype was developed based on the proposed actual-size gage (1 cm^2) to eliminate several difficulties in fabricating the final version such as availability of sensors, method of attachment, and method of cutting the thin-film pattern. Three different thicknesses of 10X prototypes were used to perform preliminary tests on the gage capabilities. Steady and unsteady measurements were made in low velocity wind tunnels. The skin friction was determined by comparing the gage output to a static calibration curve which was obtained by hanging weights to the sensing element. The thin-film measurements were compared to results obtained from side-by-side measurements of skin friction made with a Preston tube. Survivability tests in a supersonic flow, $M = 2.4$, were also performed using the 10X prototype.

The next phase of research involved the miniaturization of the thin-film gage to actual size, integrating all of the desired features into a single unit. Development of the actual-size (1X) prototype incorporated research involving miniature fabrication of the thin-film surface and sensing elements, and the design of feed-through leads to obtain

the gage output. Once the 1X thin-film prototype was developed, the gage was statically calibrated to make skin-friction measurements in subsonic and supersonic flows. Finally, survivability tests in supersonic flow, $M = 3$, were performed with the 1X prototype to demonstrate that the thin-film gage could withstand a supersonic environment.

Chapter 2

LITERATURE REVIEW

The need to accurately predict the frictional drag of a fluid passing over a surface developed over a century ago to estimate the performance of ships. The direct measurement of skin friction by Kempf [1] and Schoenherr [2] was critical in the development of skin-friction estimation for incompressible flows. The development of the jet engine in the late 1930's and early 1940's quickly brought about the need to measure skin friction in compressible flows. The effects of flow turbulence, large pressure gradients, and three-dimensional disturbances increased the difficulty in obtaining reliable estimations of skin friction in compressible flows. Many techniques have been developed to accurately measure the relatively small wall shear stresses in fluid flows. These devices must separate the very small shear forces from the dynamic pressure forces which are two orders of magnitude larger (Brown and Joubert [3]). For example, on a $q = 1000$ psf trajectory, a typical skin-friction coefficient, $C_f = 0.002$, implies surface shear forces of 2 psf. In addition, forces resulting from inertial acceleration of the skin-friction gage can be three orders of magnitude larger than the shear forces (Winter [4]).

The measurement of skin friction can be divided into two main categories: direct and indirect. The direct measurement techniques measure the applied force of the fluid to a wall element. These methods are ideal because they do not depend directly on fluid properties of the flow. This advantage is offset by numerous problems in implementing the gage. Indirect methods consist of either wall similarity techniques or momentum balance techniques. Similarity methods infer skin friction from either the size and shape of the velocity profile, or the amount of thermal transfer from the flow near the wall. Momentum techniques determine the skin friction from measurements of integral quantities of the flow, i. e., pressure gradient or momentum thickness.

INDIRECT METHODS

The velocity profile near the wall consists of a linear viscous sublayer region along the wall, a mixing region, and a logarithmic, or "law-of-the-wall" region. Clauser [5] recognized that for turbulent boundary layers the viscous sublayer has a velocity scale, u, which is the friction velocity, u^*. If constant shearing stress is assumed in the viscous sublayer, the velocity distribution is given by

$$\frac{u}{u^*} = \frac{yu^*}{v} \qquad [2.1]$$

where u is the fluid velocity at some distance y from the wall. From this relationship the friction velocity, and therefore the frictional coefficient, can be determined. The Clauser charts were originally developed for incompressible flows, but the same method can also be applied to compressible flows.

Preston [6] realized that by obtaining a single pressure measurement near the wall, the skin friction can be inferred from the relationship

$$\frac{\tau_w d^2}{4\rho v^2} = \mathrm{F}\left[\frac{\Delta P_p d^2}{4\rho v^2}\right] \qquad [2.2]$$

where the function F can be obtained from fully developed pipe flow measurements. The pressure measurements are obtained at a known distance from the wall using small diameter (0.03 in. to 0.75 in.) pitot tubes. The Preston tube relations rely on the assumption of a universal law-of-the-wall for the velocity profile for a fully turbulent boundary layer. The large numbers of tube sizes and pipe flow calibrations result in an array of calibration equations (McAllister et al. [7]). The most universal calibration equation, covering a wide range of tube sizes and flow conditions, is given by Patel [8].

Similar to the Preston tube in principle, the Stanton tube consists of a pitot tube with a rectangular opening. A Stanton tube can easily be fabricated by placing a piece of razor blade over a static pressure hole. Schematics of the Preston tube and Stanton tube are shown in Figs. 1 & 2. Since any flow disturbances which would effect the velocity profile would result in measurement error, pressure gradients and three dimensional flow disturbances must be compensated for when using either the Preston or Stanton tubes. Frei and Thomann [9] demonstrated the calibration of Preston tubes when used in turbulent flows with severe pressure gradients.

The sublayer fence also relies on the velocity profile assumption and measures the pressure difference across the fence as it protrudes into the viscous sublayer. Increased sensitivity of the sublayer fence due to the relatively large pressure difference generated across the fence, as compared to the Preston tube, and its small size allow the fence to remain within the sublayer. Consequently, the skin-friction measurements obtained

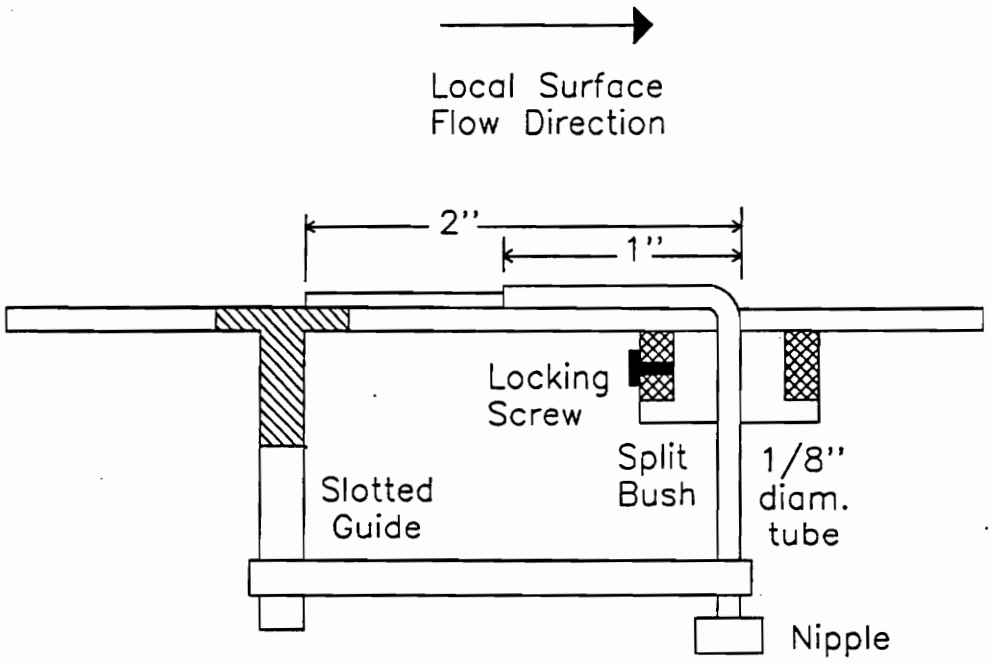

Figure 1. Schematic of Preston tube (Preston [6]).

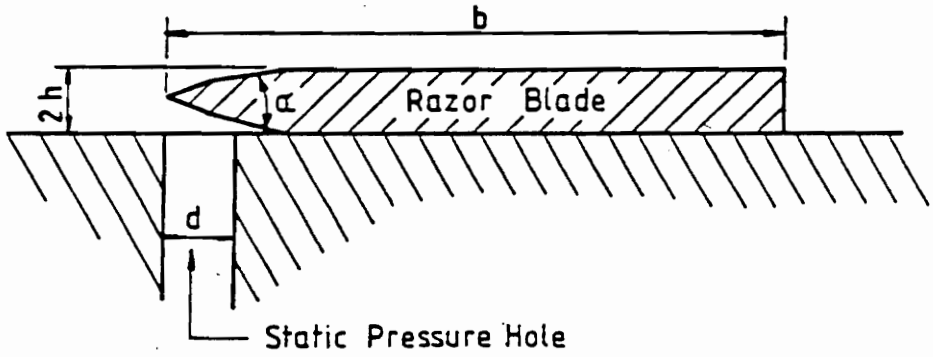

Probe Height h	mm	Angle α Degrees
A	0.05	19
B	0.115	15
C	0.130	12
D	0.330	21

Probe Scale
d = 0.6h
b = 30h
Probe Width = 90h

Figure 2. Schematic of Stanton tube (Hooper and Irrgang [11]).

from the fence are relatively insensitive to pressure gradients and other flow parameters which effect the velocity profile.

The various indirect methods of obtaining skin friction from turbulent boundary layer flows which have been discussed all rely on inferring wall shear stress from the size and shape of the velocity profile. Although compensation for flow disturbances and probe size must be considered, these devices have been widely used with confidence in steady flows. More complete reviews of these methods are given by Winter [4], Nitsche et al. [10], Hooper and Irrgang [11], and Haritonidis [12].

Momentum techniques differ from similarity techniques in that measured quantities are substituted into the momentum integral equation to infer skin friction. The pressure loss, dp/dx, is measured for fully developed pipe flow, while derivatives of the momentum thickness, Θ, are measured for developing boundary layer flow. This technique is limited by the difficulty in obtaining accurate measurements of the desired quantities, especially in three-dimensional flows with severe pressure gradients (Brown and Joubert [3]).

Another indirect method is to infer the skin friction from the heat transfer from a heated surface element. This technique was first investigated by Fage and Faulkner [13] and hot-wire skin-friction gages, based on the heat-momentum analogy between skin friction and heat transfer, were tested by Ludweig and Tillman [14] and Liepman and Skinner [15]. Improvements on this technique were made by Bellhouse and Schultz [16, 17] when they designed a hot-film skin-friction gage. The hot element consists of either a thin wire embedded in the surface, or a thin film which is deposited on a substrate mounted to the surface. The principle of operation of the hot-film skin-friction gage is similar to that of a hot-wire anemometer. The electrical power, e, supplied to the gage is related to the skin friction, τ , by the equation

$$\frac{e}{\Delta T} = A + B(\rho\tau)_w^{1/3} \qquad [2.3]$$

where ΔT is the temperature difference between the hot element and the fluid, and A and B are constants which are mildly dependent on ΔT.

Errors result in heat transfer methods because of the reduced flow velocities near the wall. This results in conduction through the fluid which can cause errors in unsteady flow measurements. A second source of error is the conduction of heat through the substrate. The heat transfer in the substrate results in an increased heating length because the heated section is greater than the actual thin-film element. This increased heated length effects the thermal boundary layer which determines the local heat flux, and therefore, the measured skin friction. Although the effective length of the hot-film can be accounted for by calibration in steady flows, the phase and amplitude of the measured skin friction can be greatly in error in unsteady flows (Diller and Telionis [18]). Mechanical position of the hot element can also be a source of error in skin-friction measurement. If the hot element is not mounted flush with the wall surface significant errors, on the order of 30%-40%, can result (Lefebvre and LaPointe [19]). Complete reviews of heat transfer methods to measure skin friction are given in Hanratty and Campbell [20] and Diller and Telionis [18].

Hot element probes are the most popular skin-friction measurement devices partly because of their high frequency response which allows frequency spectra in unsteady flows. Difficulties arise, however, in the calibration of thin-film gages because of the relatively slow thermal response of the substrate. The problems with unsteady calibration, and the proper use of these instruments in unsteady flows, is detailed in many articles (e.g., Cole and Black [21], Menendez and Ramprian [22], Bellhouse and Schultz [16, 17], Nandy and Tarbell [23], Cook and Giddings [24]).

The final indirect skin-friction measurement technique pertains to liquid tracers. This classification consists primarily of oil tracers and liquid crystals. The skin friction acting on a surface is proportional to the streak length resulting when an oil dot is placed

on the surface. Time-averaged techniques for measuring the thickness of a liquid film on a surface due to convection have also been developed. Monson [25] used laser interferometry to optically measure the thickness of an oil film on a surface in three-dimensional flows. Liquid crystals are another surface coating technique in which shearing stresses acting on the surface cause changes in the way white light is scattered by the crystals (Klein and Margozzi [26, 27]).

DIRECT METHODS

Early work on developing a direct measurement of skin friction in compressible flows was done be Schultz-Grunow [28] and Dhawan [29]. Direct measurement of the small skin-friction forces relative to pressure and inertial forces is complicated by a number of factors. A number of these problems are listed below. (Winter [4])

1. Provision of a transducer for measuring small forces or deflections, and the compromise between the requirement to measure local properties and the necessity of having an element of sufficient size that the force on it can be measured accurately.
2. The effect of the necessary gaps around the floating element.
3. The effects of misalignment of the floating element.
4. Forces arising from pressure gradients.
5. The effects of gravity or of acceleration if the balance is to be used in a moving vehicle.
6. Effects of temperature changes.
7. Effects of heat transfer.
8. Use with boundary-layer injection or suction.
9. Effects of leaks.

10. Protection of the measuring system against transient normal forces during starting and stopping if the balance is to be used in a supersonic tunnel.

The floating element balances consist of a floating head attached to an arm on which the sensing is done. The vast majority of these arms consist of a single cantilever beam or a parallel linkage device. When the head is loaded during gage operation, the skin-friction measurement is obtained from the sensing arm by either measuring the head displacement or the amount of force needed to keep the head in a stationary position. The displacement balance usually employs a linear variable displacement transducer (LDVT) to sense the bending strain in the sensing arm. The feedback balance operates with a Kelvin current balance or a coil and permanent magnet to obtain the force acting on the sensing arm. A complete review of the direct force balance development is given in Winter [4].

The relatively large size of the floating elements result in large gap sizes and low frequency response. Therefore, these devices do not have the capability of making detailed time-resolved measurements of skin friction, although time-averaged measurements have been made. The necessary gaps around the floating element, and misalignment effects have been studied in detail by Allen [30, 31]. Gap to head diameter, g/D, and lip to head diameter, c/D, can be a significant source of measurement error in these devices. To eliminate gap and misalignment effects, Schmidt et al. [32] has shown that gap size can be reduced by an order of magnitude through microfabrication techniques. Their floating element, shown if Fig. 3, was fabricated from polyamide and the element movement is detected by a differential capacitance technique. This sensing technique makes the skin-friction measurement insensitive to normal forces acting on the floating element. The extremely small size of the element results in a frequency response to 20 kHz which allows the measurement of transient fluctuations in skin friction.

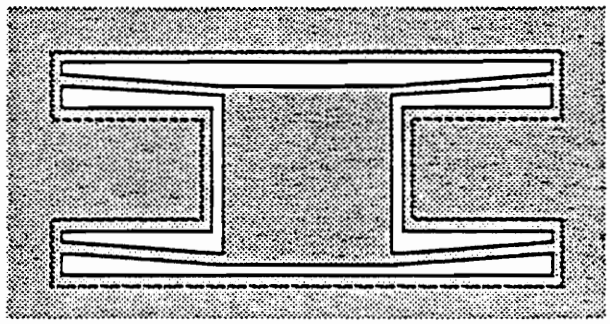

(a)

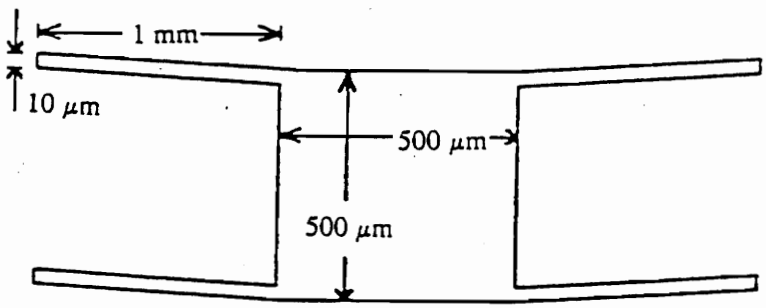

(b)

Figure 3. (a) Top view of micromachined floating element under shear load, (b) dimensioned drawing (Schmidt et al. [32]).

Nitsche et al. [33] have also obtained similar frequency response using piezo-electric foils.

Several skin-friction balances have been developed for use in moderately low temperature, supersonic flows as discussed in articles by Allen [30], Voisinet [34], Roensch and Cadwell [35], and Bruno and Risher [36]. The task of measuring skin friction in the hostile environment present in supersonic combustion flow has been addressed by Orth et al. [37] and DeTurris et al. [38]. Typical combustion flow operating conditions are static temperatures of 1100-2200 K, and static pressures of 0.5-1.0 atm. The gage developed by DeTurris, shown if Fig. 4, consists of a floating element attached to a cantilever arm, on which crystal strain gages are mounted. Bending of the arm due to shear forces creates stresses in the arm which are detected by the strain gages. Active cooling of the cantilever arm reduces error resulting from a temperature difference between the floating element and sensing unit. Measurements were taken for a combustion flow condition of $M = 3.0$ and static temperature and pressure of 860 K and 0.42 atm.

The proposed direct-force-reading, thin-film skin-friction gage is designed to operate in a variety of flow conditions, including hostile supersonic combustible flows. The ability to make accurate high frequency measurements (> 1 kHz) in unsteady flows is a major reason in pursuing the thin-film concept for measuring skin friction. The small unit size, mounting the sensing elements on the wall surface to match the thermal environment, no active cooling requirements, and having virtually no acceleration effects because of the extremely small mass of the thin film, are also potentially significant advancements to existing skin-friction measurement devices.

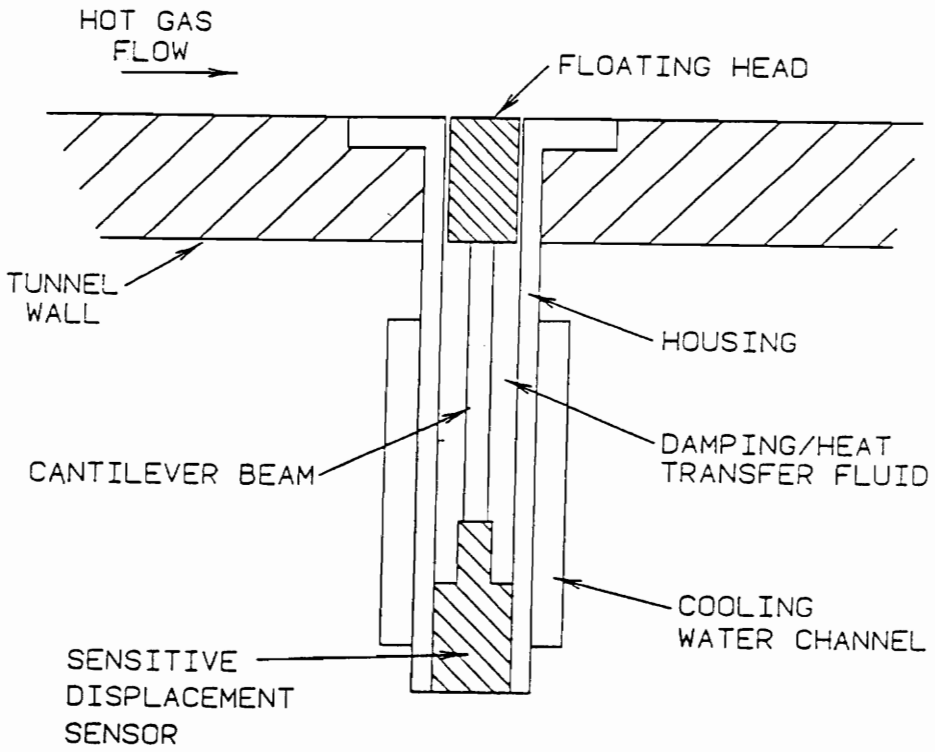

Figure 4. Schematic of cantilever beam, floating element skin-friction gage (Deturris et al. [38]).

Chapter 3

THIN-FILM CONCEPT FOR MEASURING SKIN FRICTION

Measuring shear forces acting on a thin film mounted flush with the wall surface offers a variety of advantages over current skin-friction measurement techniques. The thin-film capabilities are:

- Direct skin-friction measurements ranging from approximately 10 - 2700 N/m^2 (0.0015 - 0.4 $lb/in.^2$)
- High frequency response ($>$ 5 kHz) for non-steady measurements
- High temperature measurements (800 K wall temperature)
- Full 360° directional sensitivity for measurement of three-dimensional and reversing flows.

Although current skin-friction measurement technology achieves some of these desired capabilities, no single gage currently exists which can perform all the desired functions. The potential for the thin-film gage to incorporate all the desired functions into

a single unit for the accurate prediction of skin friction in both subsonic and supersonic flows, including a scramjet environment, makes this a very attractive device.

THIN-FILM GAGE OPERATION PRINCIPLE

The basic concept of the thin-film skin-friction transducer is the direct measurement of strain in a linear material resulting from an applied shear load. The shear forces act on an active floating element surface (1 cm^2) which is constructed from a metal film such as nickel. The resulting strains are concentrated in four strain tabs which have a small width (0.25 mm) as compared to the active element, see Fig. 5. The shear force, F_s acting on each strain tab resulting from the shear, τ_w, on the active surface can be calculated as

$$F_s = \frac{\tau_w A_{gage}}{2} \qquad [3.1]$$

where A_{gage} is the active surface area. The factor of two in Eq. 3.1 accounts for the shear loading on the active surface distributed to two strain tabs along each axis of the thin-film gage. The change in strain, $\Delta\varepsilon$, in each tab resulting from the shear force is calculated as

$$\Delta\varepsilon = \frac{F_s/A_c}{E} \qquad [3.2]$$

where A_c is the tab cross-sectional area, and E is the modulus of elasticity. Substituting Eq. 3.1 into Eq. 3.2, the change in strain in each tab resulting from the shear stress acting on the active surface is given by

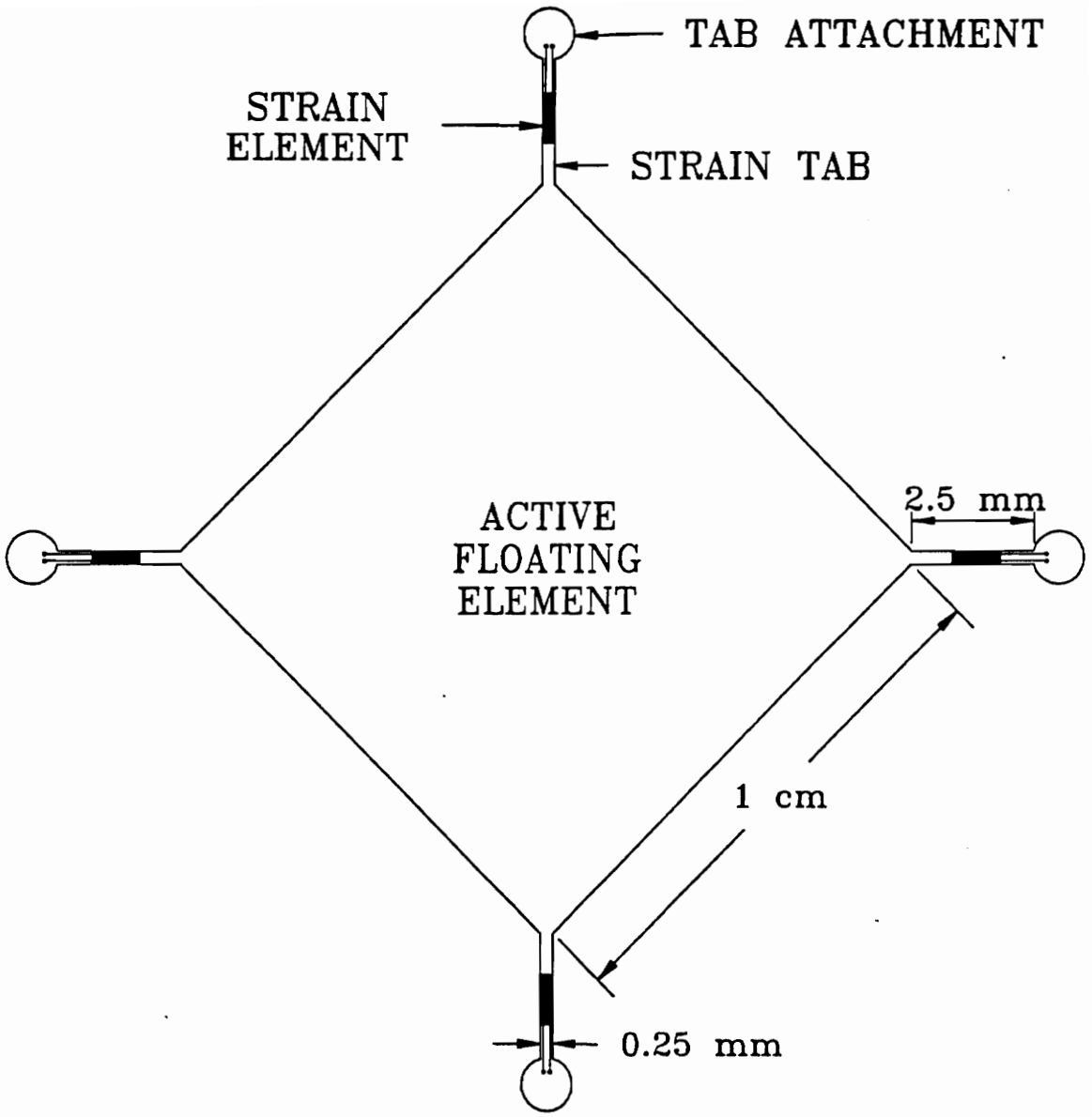

Figure 5. Thin-film skin-friction gage

$$\Delta\varepsilon = \frac{\tau_w}{2E}\left(\frac{A_{gage}}{A_c}\right). \qquad [3.3]$$

A positive change in strain is associated with tension forces acting on a strain tab, while a negative change in strain results from compression of a strain tab.

A sensing element is located on each strain tab to measure the strain resulting from the shear load. The ends of the strain tabs are enlarged to facilitate the attachment of the thin film to the wall. The tab ends are attached to the wall so that the strain tabs are preloaded in tension to ensure uniform strains in the tabs. This method of attachment allows the active surface and strain tabs to move freely when a shear load is applied.

The small thickness of the thin film (25 μm) allows a sufficient gage sensitivity to measure the relatively small shear forces acting on the active surface. For example, for a 10 N/m^2 shear acting on the 1 cm^2 thin-film surface, a shear force of 0.010 N can be measured. The wide range of possible skin-friction measurements (10 - 2700 N/m^2) includes both subsonic and supersonic flow regimes. The lowest shear measurement for a nickel thin-film gage is calculated from Eq. 3.3 based upon the assumption that the smallest measurable change in strain in each tab is 1 $\mu\varepsilon$. The maximum shear measurement corresponds to the shear force which results in 30% of the yield stress of the strain tabs.

The active element and sensing elements must exhibit specific physical properties to function in their desired capacity. The active element must have a high thermal conductivity to maintain the thin-film temperature near the wall temperature to match the thermal environment of the wall. The material must also withstand high temperatures (800 K) which are present in a scramjet environment. Metals such as nickel have

a melting point of 1730 K which allow them to be used in high temperature environments.

Strain gages are used as the sensing elements, therefore, they must be electrically conductive. A small current is applied to the strain gage to relate a change in resistance of the strain gage to the strain in the thin-film strain tabs. The tab strains resulting from the shear loading of the active surface cause a change in resistance of the strain gages given by

$$\Delta\varepsilon = \frac{\Delta R/R}{\mathrm{GF}} \qquad [3.4]$$

where GF is the gage factor of the strain gage. The gage factor is a geometric property which is a function of the cross-sectional area change, $\Delta A/A$, of the strain element when the material is strained. The sensitivity of the strain gage is solely a function of the gage factor. The thermal properties of the sensing elements should match those of the active element, so ideally the same material should be used to construct the entire thin-film gage. By matching the thermal expansion characteristics of the sensing elements with the active element, maximum temperature compensation is achieved.

A thin layer of fluid is placed under the thin film to maintain the active element temperature near the wall temperature. The fluid layer increases the heat transfer from the thin film to the wall, and it also prevents air from flowing under the active element. Air flow penetrating beneath the thin film can result in thermal insulation of the gage, increased shear loads, and the ultimate failure of the thin-film gage caused by lifting of the thin-film into the flow. The thin film must be maintained near the wall temperature to keep the gage below the melting temperature of the thin film and to limit the high temperature effects on strain measurements. The thin-film temperature, T_{gage}, can be easily calculated by the following relation

$$T_{gage} = T_{wall} + \frac{q''\delta_f}{k_f} \qquad [3.5]$$

where δ_f is the fluid layer thickness, and k_f is the fluid thermal conductivity. The thin-film temperature is assumed to be uniform for a maximum wall temperature of 400 K. The effects of varying fluid layer thickness on the thin-film temperature is illustrated in Fig. 6. The thin-film temperature as a function of varying fluid layer thickness is given for a heat flux, q″, of 4.1 MW/m² (2.5 BTU/in.² sec) and for several fluids with a variety of thermal conductivities. The heat flux into the wall is a result of convection and radiation from the combustion flow.

MICROFABRICATION OF THE THIN-FILM SENSOR

The strain gages used as the sensing elements can be sputter-coated directly onto the strain tabs. This technique involves sputtering a thin insulation layer onto the strain tab surface. The pure metal strain sensor is then layed down with a protective ceramic layer covering the strain sensor to protect the sensing element from the potentially destructive scramjet environment. The thickness of the entire strain sensor is on the order of a few microns. This allows the sensing element to be mounted on the thin-film strain tabs without affecting the local stiffness of the strain tabs. The microfabrication techniques necessary for the development of the thin-film skin-friction gage were developed for a heat flux microsensor (Hager et al. [39]).

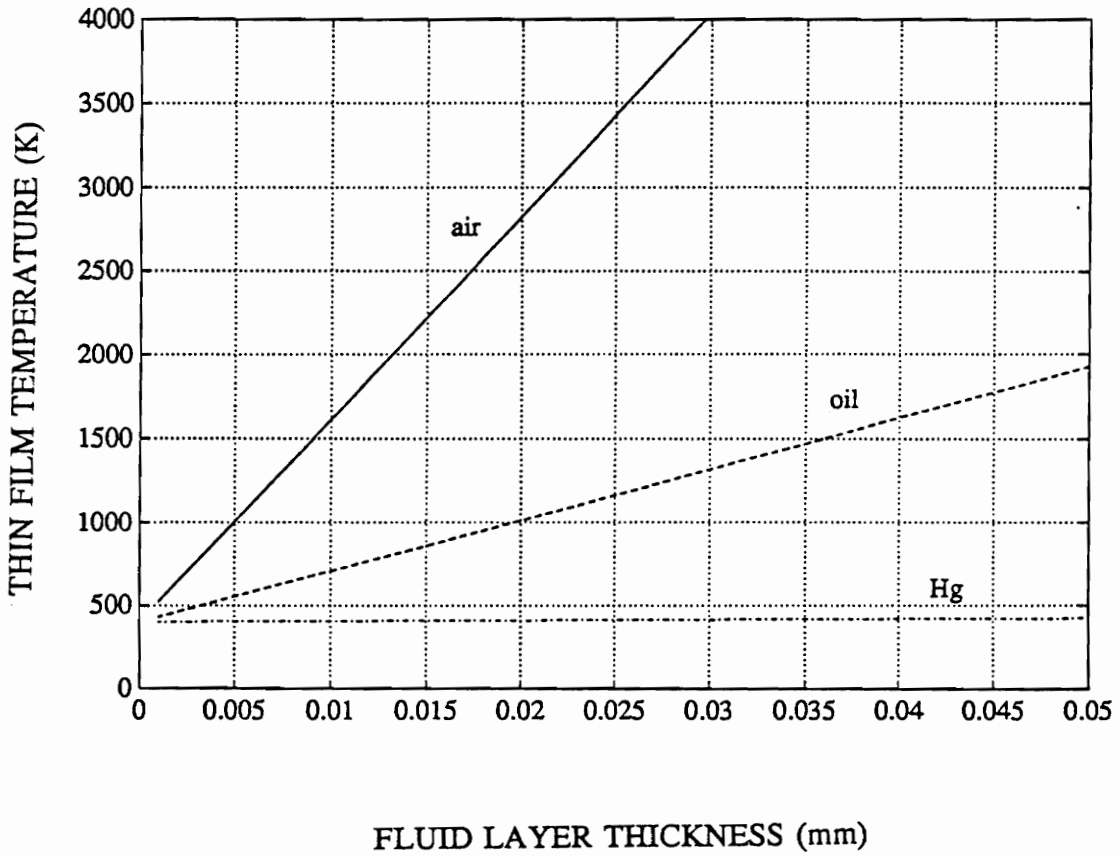

Figure 6. Calculated thin-film gage temperature for fluids with varying thermal conductivity and constant wall temperature of 400 K.

A thermocouple can also be sputtered onto the strain tabs for temperature compensation. Non-uniform temperature across the thin-film surface can result in thermal effects on the resistance of the strain sensors. These effects can be compensated for by monitoring the temperature of each individual tab. Temperature compensation is also needed for high temperature strain measurements. The strain sensor sensitivity may change at elevated temperatures because of changes in gage factor and electrical resistance of the strain sensor. Therefore, the temperature of the thin film should be monitored. The uniform, high temperature compensation is anticipated to be small, however, relative to the thermal effects (non-uniform) resulting from varying temperatures of individual strain sensors.

The extremely small size of the sensing elements makes the microfabrication techniques previously discussed ideal for developing the thin-film gage. The entire thin-film gage thickness is of the order of 25 μm (0.001 in.) so no flow disruption occurs as a result of flow passing over the gage. Sputtering the sensing elements onto the strain tabs also allows the sensor size, sensor sensitivity, and gage material properties to be chosen to optimize the thin-film gage capabilities. Fabricating the sensing element directly onto the thin-film surface also eliminates high temperature problems such as adhesive failure between the sensing elements and thin film.

WHEATSTONE BRIDGE CIRCUITRY

Leads connect each strain sensor to a Wheatstone bridge circuit. The strain gages can be mounted on the backside of the thin film, allowing the strain sensors and leads to be completely shielded from the combustion flow. The set of strain gages along each

axis of the thin-film gage are connected to a separate half-bridge circuit. The independent measurement of shear forces acting along each axis of the gage allows for the 360° directional sensitivity of the thin-film gage. The output of the streamwise and crosswise axes can be added vectorially to determine the flow direction.

The set of strain sensors along each axis of the thin-film gage are connected in adjacent arms of a Wheatstone bridge, see Fig. 7. The other two arms contain fixed 1000 Ω resistors to complete the half-bridge configuration. The advantages of output linearity, uniform bending/temperature compensation, and differential output of the strain sensors along each axis are obtained by arranging the strain gages in this configuration. Certain configurations of a Wheatstone bridge are nonlinear, for example, a quarter bridge. For certain half-bridge and full-bridge configurations with small changes in resistance relative to the actual strain gage resistance, however, the bridge output , E_{out}, can assumed to be linear and is given by

$$E_{out} = \frac{E_{in}}{4}\left[\frac{\Delta R_1}{R_1} - \frac{\Delta R_2}{R_2}\right] \qquad [3.6]$$

where E_{in} is the applied voltage across the bridge. The half-bridge configuration gives linear output of the thin-film gage resulting from the changes in strain of the thin-film tabs caused by the shear loading.

The shear forces acting along each axis of the thin-film gage result in axial tension forces in one tab, while axial compression forces exist in the opposite tab. The strain sensors are placed in adjacent arms of the bridge circuit to provide a differential output of the strain signals. Strains resulting from tension forces result in positive resistance changes of the strain sensors (ΔR_1) , while compressive forces result in negative changes in resistance ($-\Delta R_2$). Therefore, using Eq. 3.6, the bridge output is obtained from

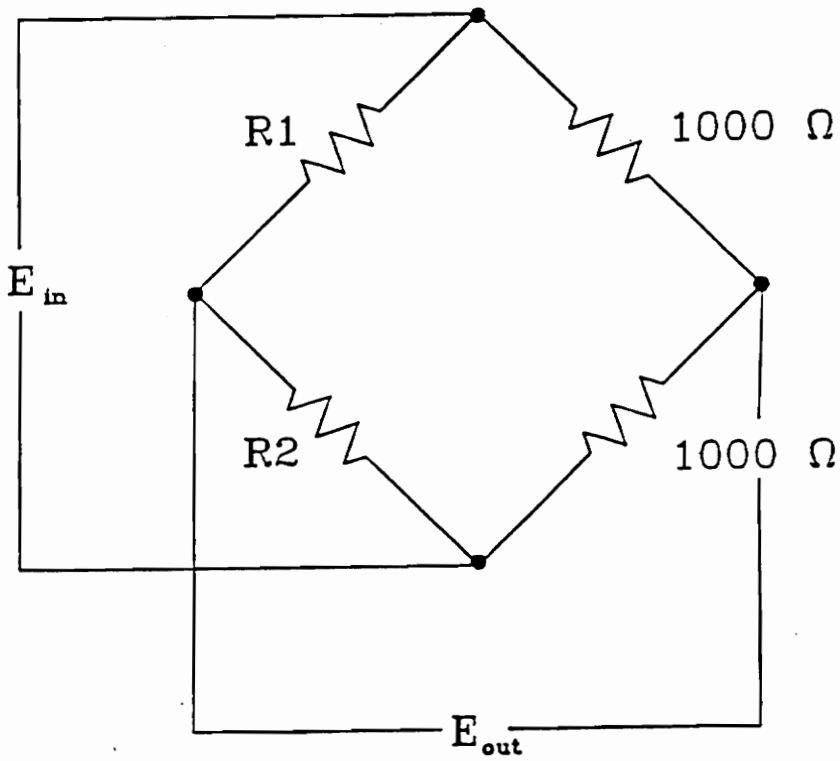

Figure 7. Wheatstone bridge in half-bridge configuration for cancellation of uniform temperature and bending effects.

$$E_{out} = \frac{E_{in}}{4}\left[\frac{\Delta R_1}{R} - \frac{-\Delta R_2}{R}\right] \qquad [3.6a]$$

where $R = R_1 = R_2$. This bridge arrangement allows strains to be sensed resulting from shear forces acting along each axis of the thin-film gage.

The half-bridge configuration allows cancellation of equal strains in the strain tabs resulting from uniform thermal or uniform bending effects. A uniform temperature change of the thin film results in a uniform expansion or contraction of the thin film. The strain tabs on opposite sides of the gage are strained in the same manner, therefore, the strain sensors undergo an equal resistance change of the same sign. The differential output of the bridge circuit, given in Eq. 3.6, results in the cancellation of the uniform strains. Strains resulting from uniform bending of the thin film, caused by normal pressures, are cancelled in the same manner.

The half-bridge arrangement with the sensing elements placed in adjacent arms of the bridge allows the measurement of strains resulting from shear loading of the thin film. These strains are separated from uniform strains on the thin film which are cancelled by the bridge circuitry. Other sources of strain, such as non-uniform temperature effects and torsional straining of the strain tabs, can not be eliminated by this specific bridge arrangement. These effects are minimized by externally compensating for non-uniform temperature effects and by minimizing torsional straining of the strain tabs.

The two fixed resistors in the bridge circuit and the strain sensors each have a 1000 Ω resistance. High resistance strain sensors are used in the bridge circuit to minimize the power dissipated by the strain gages by reducing the current through the gages. The lower power levels supplied to the strain gage resistors result in reduced thermal heating of the sensors. This minimizes the thermal effects on the thin-film gage output when the strain sensors are subject to convective flows.

THIN-FILM FREQUENCY RESPONSE

Detailed time-resolved measurements of skin friction in unsteady flows can be made with the thin-film gage because of its high frequency response. The frequency response of the thin-film gage is obtained by modelling the thin film as an axial loaded rigid body. The natural frequency, f_n, of the thin film is given by

$$f_n = \frac{1}{2\pi}\sqrt{\frac{k}{m}} \qquad [3.7]$$

where m is the mass of the active element and k is its stiffness. Assuming all the thin-film deformation occurs in the tab lengths, L, when loaded by the shear flow, the stiffness of the thin-film gage can be calculated as

$$k = \frac{2A_cE}{L}. \qquad [3.8]$$

The factor of two included in the numerator of Eq. 3.8 accounts for tabs attached to both ends of the thin film. Substituting Eq. 3.8 into Eq. 3.7, the thin-film natural frequency is given by

$$f_n = \frac{1}{2\pi}\sqrt{\frac{2A_cE}{Lm}}. \qquad [3.9]$$

For a 1 cm², nickel, thin-film gage, with a thickness of 0.025 mm (0.001 in.) and the dimensions given in Fig. 5 on page 19, the natural frequency is calculated to be 34 kHz.

The fluid layer beneath the thin-film active surface acts as a fluid damper resulting from the viscous shearing of the fluid as the active surface translates under a shear load. The damping coefficient, c, of the fluid is given by

$$c = \frac{\mu_f A_{gage}}{\delta_f} \qquad [3.10]$$

where μ_f is the absolute viscosity of the fluid. The damping ratio, ζ, is calculated as

$$\zeta = \frac{c}{c_{cr}} = \frac{c}{2\sqrt{km}} \qquad [3.11]$$

where c_{cr} is the critical damping.

The nondimensional expressions for the amplitude and phase of the thin-film gage response as a function of the normalized frequency, ω/ω_n, are given by

$$\frac{Xk}{F} = \frac{1}{\sqrt{\left[1 - \left(\frac{\omega}{\omega_n}\right)^2\right]^2 + \left[2\zeta\left(\frac{\omega}{\omega_n}\right)\right]^2}} \qquad [3.12]$$

$$\phi = -\tan^{-1}\left[\frac{2\zeta\left(\frac{\omega}{\omega_n}\right)}{1 - \left(\frac{\omega}{\omega_n}\right)^2}\right] \qquad [3.13]$$

where Xk/F is the normalized amplitude and ϕ is the phase angle. Normalized frequency is the ratio of natural frequency to forcing frequency, while the normalized amplitude is the ratio of input amplitude to response amplitude. Assuming a .005 mm layer of oil under a 1 cm² nickel thin-film gage, 6% critical damping results from the fluid layer. Figure 8 shows the normalized frequency response and phase angle of the thin-film gage with a damping ratio of 6%. Assuming a flat response amplitude to 20% of the natural frequency (34 kHz), the useful frequency response is 7 kHz.

The sample calculations illustrated throughout this chapter demonstrate the capabilities of the thin-film concept. Although these calculations are only estimates of the

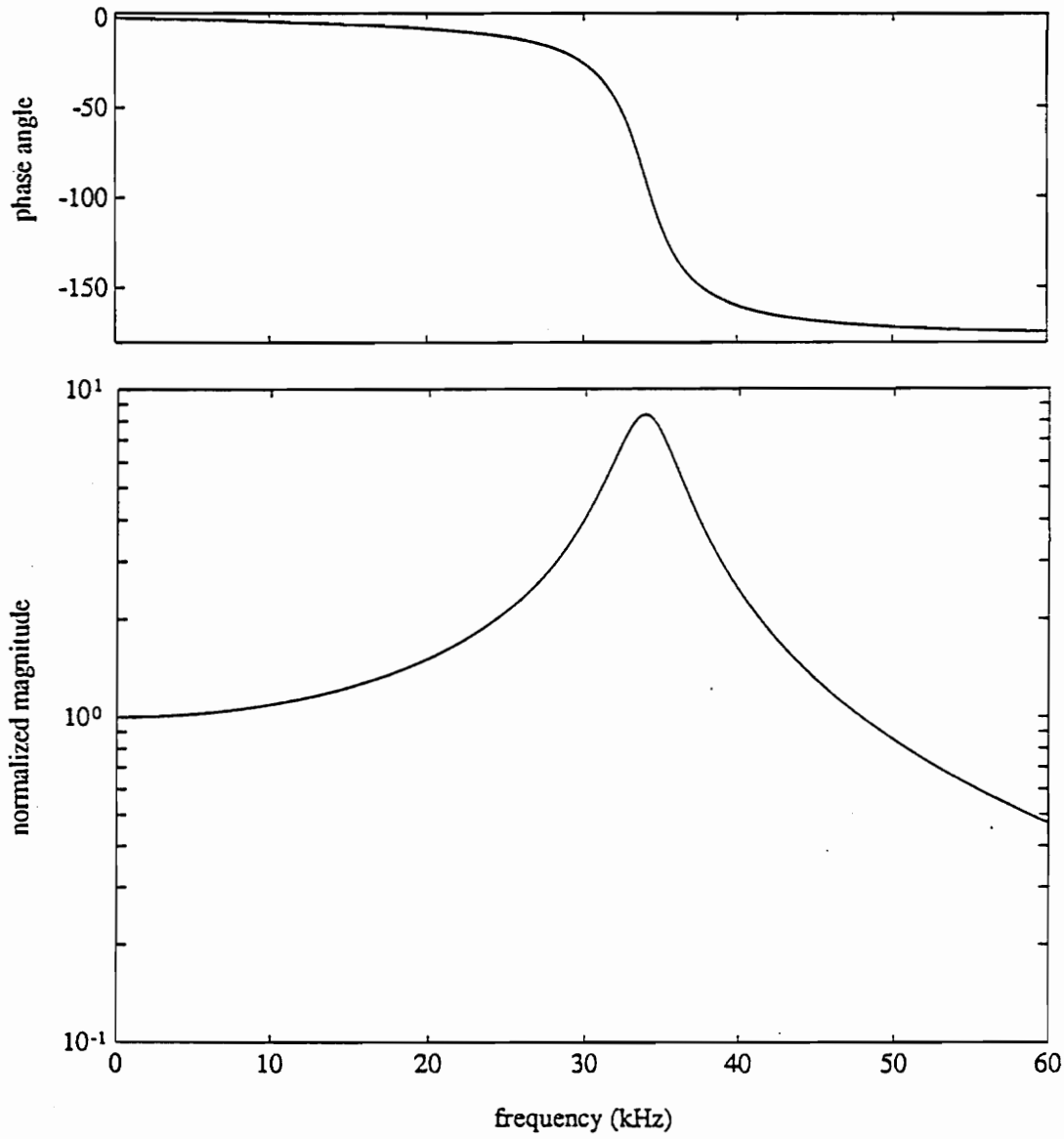

Figure 8. Frequency response of 1 cm x 1 cm nickel thin film gage with natural frequency of 34 kHz and 6% critical damping.

actual thin-film performance, they illustrate the enormous potential of the thin-film concept over existing skin-friction measurement technology. The following chapters describe the testing performed to demonstrate the thin-film capabilities, and to incorporate these characteristics into a single unit.

Chapter 4

DEVELOPMENT OF THE 10X PROTOTYPE THIN-FILM GAGE

To test the initial concept of the thin-film skin-friction gage, a 10X scale prototype was constructed. The initial prototype was made to a large scale to facilitate the thin-film gage fabrication and the attachment of the thin film to the wall surface. This also allowed readily available commercial strain gages to be used as the sensing elements. The 10X prototype could be constructed in a relatively short time period compared to an actual-size thin-film gage where the small size film leads to many manufacturing difficulties. The 10X prototype allowed the initial testing of the thin-film concept, and the identification of possible design flaws which could be corrected in the design of an actual size (1 cm x 1 cm) thin-film gage.

10X PROTOTYPE TEST APPARATUS

The 10X prototype was designed with all the dimensions based upon the initial thin-film concept described in Chapter 3. Three thicknesses of stainless steel shim stock were cut to form the active floating element. These thicknesses of 0.025 mm (0.001 in.), 0.13 mm (0.005 in.), and 0.25 mm (0.010 in.) were cut to provide active elements with different stiffnesses. An electrical-discharge-machine (EDM) was used to cut the thin films because of the thinness of the material and the need to cut the thin film to close tolerances. The strain tabs were cut to close tolerances to insure similar straining in each tab when the active surface was loaded. All the thin-film gages were cut simultaneously to insure all the 10X prototypes were identical.

A drawing of the 10X prototype with the critical dimensions is shown in Fig. 9. The active surface of the thin film has a shear area of approximately 100 cm^2 (4 $in.^2$), and the tab widths are 3.2 mm (0.125 in.). Holes were cut in the tab attachments so that fasteners could be used to attach the thin-film prototype to a base plate. Standard size screws, along with washers, were used to attach the thin film to the base plate.

The thin-film prototype was attached to a 0.64 cm (0.25 in.) thick aluminum base plate. The 10X prototype thin-film gage mounted on the square base plate (33 cm x 33 cm) is shown in Fig. 10. This plate served as the wall surface and allowed the attachment of the thin film with varying preload levels in the strain tabs. The preloading of the strain tabs was necessary to insure equal strains in each tab when the active element was loaded. Two adjacent tabs of the thin film were permanently fastened to the base plate, while the other two tabs were fastened to 0.16 cm (0.0625 in.) thick slide plates. These plates allowed the tension along each axis of the thin film to be adjusted independently. Weights were attached to the slide plates to set the preload in each strain tab

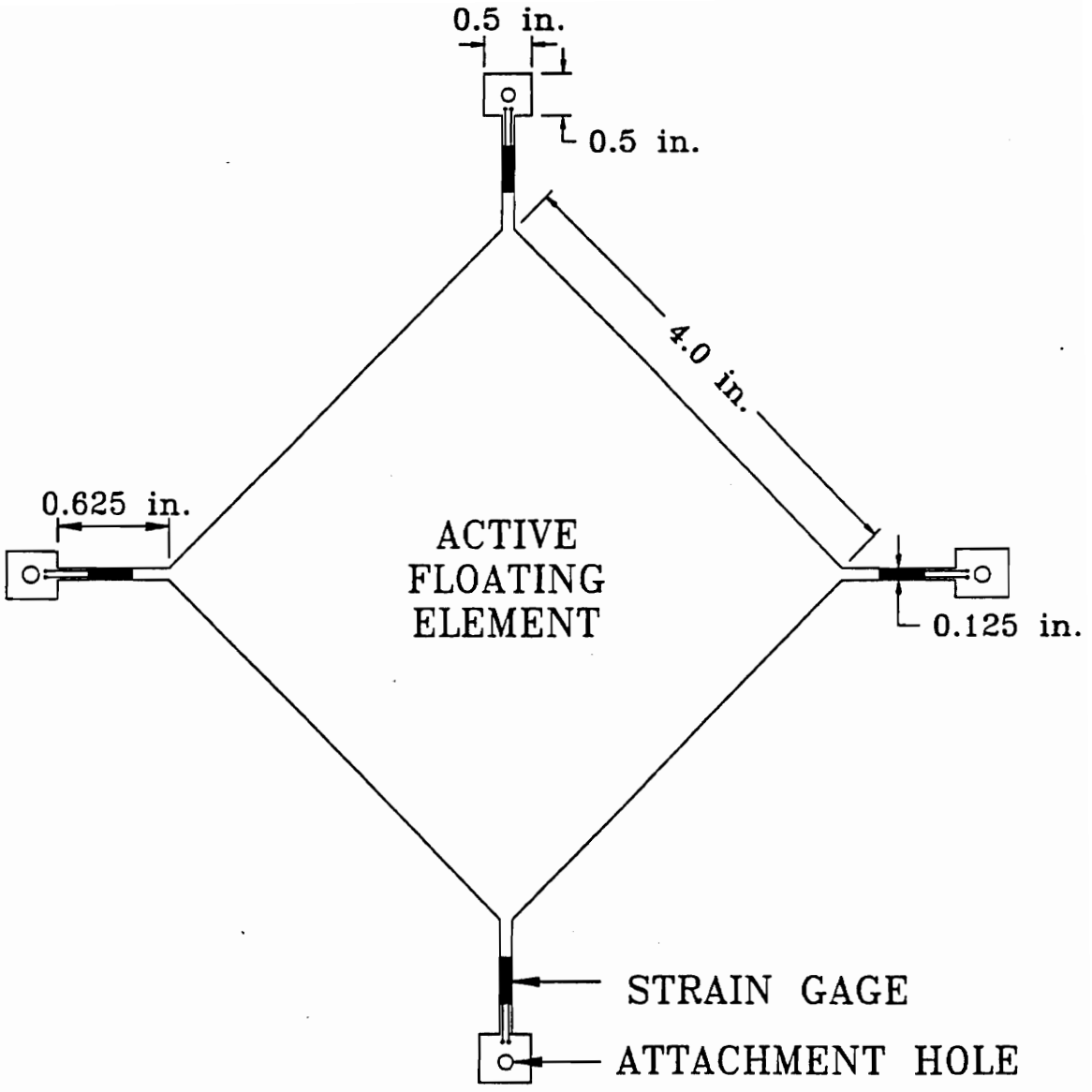

Figure 9. 10X prototype of thin-film shear stress gage.

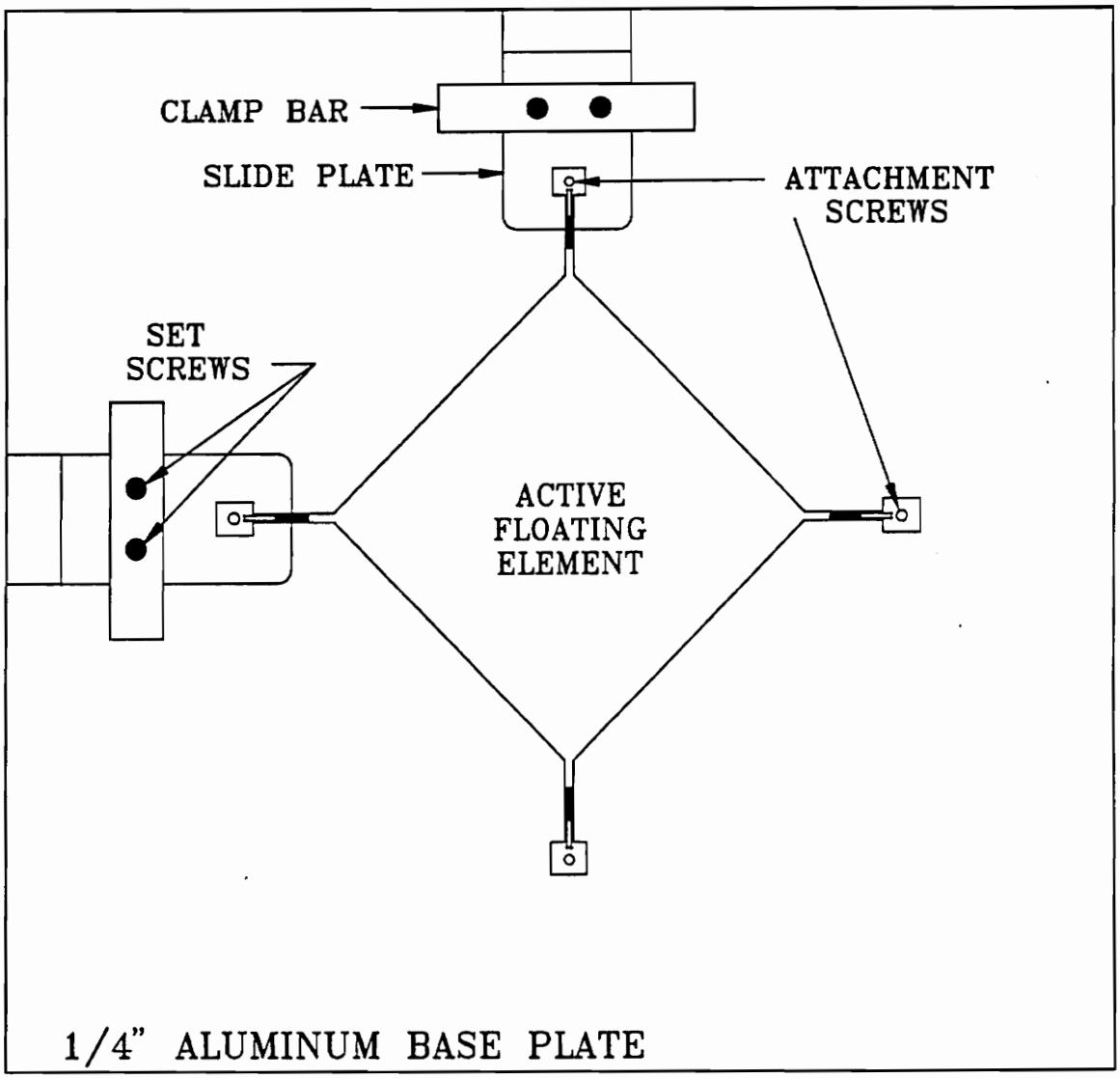

Figure 10. Baseplate assembly for 10X prototype.

at 22 N (5 lbs). The slide plates were then locked into position by tightening the set screws located in the clamp bar as shown in Fig. 10.

10X PROTOTYPE SENSING ELEMENTS

Once the thin-film gage was installed on the base plate, commercially available strain gages were installed as the sensing elements. The strain gages used were general purpose constantan strain gages with a 350 Ω operating resistance and a gage factor of 2.115 (Measurements Group, Inc., CEA-06-062UW-350). These strain gages were chosen based upon their size and operating resistance. The strain gages were mounted on each of the strain tabs and the leads from the strain gage pair along each axis of the active element were run to a separate half-bridge circuit.

The two strain gages along each axis of the active element were connected to adjacent arms of a Wheatstone bridge. This half-bridge configuration senses strains resulting from shear loading of the thin film. Strains resulting from uniform temperature and bending effects on the active element are inherently cancelled by this bridge configuration, as described in Chapter 3. The half-bridge circuit is part on an electronics package developed specifically to amplify the relatively small output of the strain gages.

ELECTRONICS

The unamplified output of the thin-film gage sensing elements is of the order of a microvolt for low shear flows. For example, Eq. 3.3 on page 20 predicts a tab strain of 120 $\mu\varepsilon$ for a 350 N/m^2 (0.05 lb/in.^{2}) shear acting on a 0.025 mm thick 10X prototype. For an input voltage, E_{in} = 5 Volts, gage resistance, R = 350 Ω, and a gage factor, GF = 2.115, Eq. 3.6, along with Eq. 3.4, predicts a bridge output voltage of 0.6 mV. Amplification of this low-level signal to a convenient level in a high noise environment is desired to obtain accurate skin-friction measurements from the thin-film gage. An electronics package, designed and built by John Putz [40] for the thin-film gage, was used to amplify the low-level signal.

The entire electronics package consists of a Wheatstone bridge, a voltage regulator, a precision instrumentation amplifier, and a four 9-V battery power supply. A schematic of the electronic circuit is shown in Fig. 11. A high precision, low noise, instrumentation amplifier was used because of the low-level output of the strain gage transducers. The Analog Devices AD624 differential amplifier was chosen because it offers (Analog Devices [41]):

- High accuracy gains up to G = 1000
- Low noise: 0.2μV p-p (0.1 to 10 Hz)
- Low gain temperature coefficient: 15ppm max (G = 1000)
- High linearity: $\pm$ 0.005% (G = 1000)
- High Common Mode Rejection: 120 dB max (G = 1000)
- Gain-bandwith product of 25 MHz.

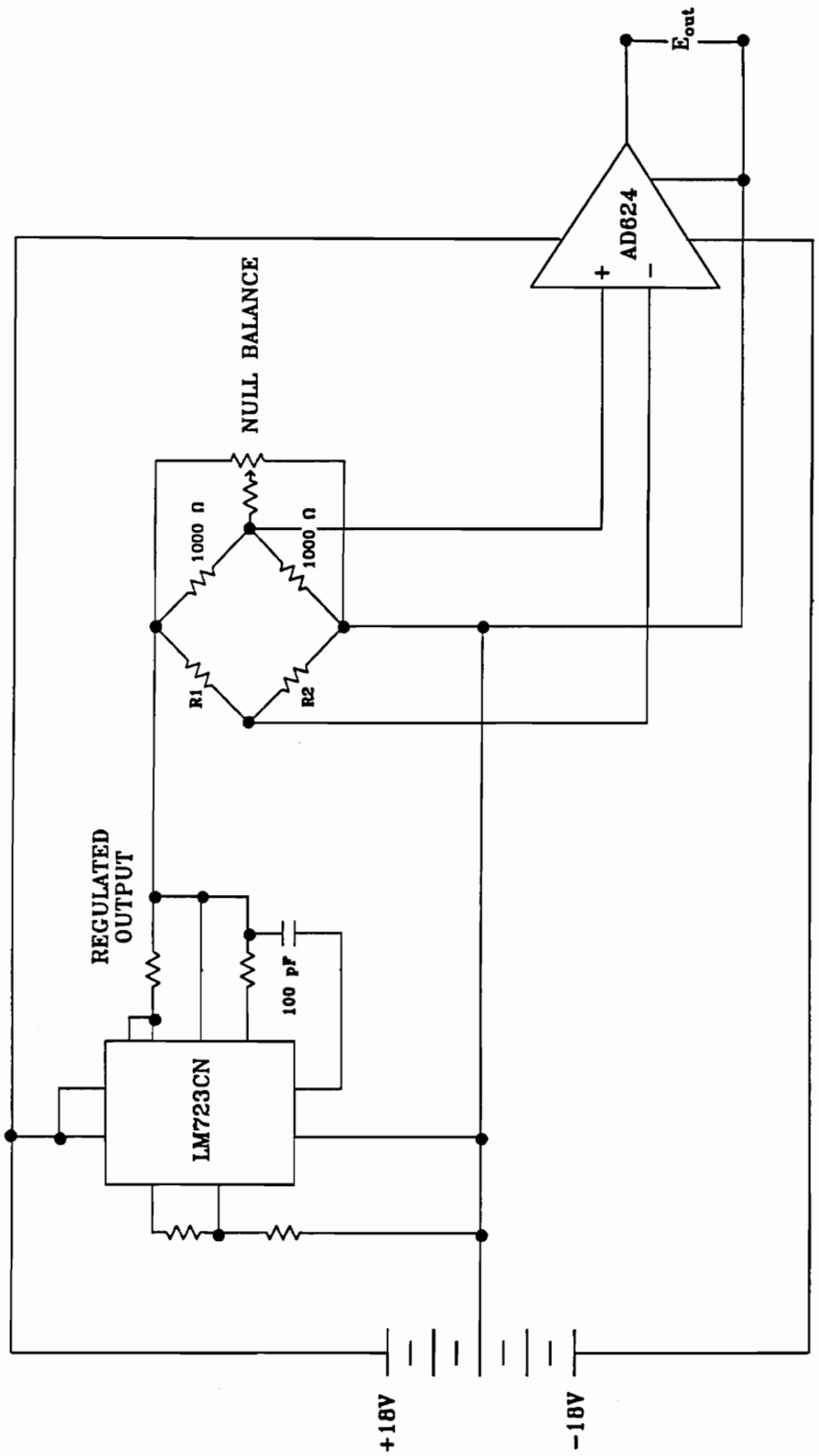

Figure 11. Schematic of electronics package for thin-film shear stress gage (John Putz [40]).

A dip switch allows variable gains of 1, 100, 200, 500, and 1000 to be set. Relative changes in output of the thin-film gage can be obtained by zeroing the bridge output with a null balance shown in Fig. 11.

A differential amplifier was used because it provides an output proportional to the difference between input voltages supplied by the pair of strain gages along each axis of the thin-film gage. This allows differential strain measurements along each axis of the thin-film gage to be made instead of absolute strain measurements. The amplifier operates in a differential mode because the two input terminals are not grounded but are floating inputs.

The high amplification of the low-level signal requires a high input impedence of the differential amplifier. High impedence amplifiers configured as voltage followers are used as inputs to the differential amplifier. This results in the entire voltage drop occurring across the amplifier input terminals, preventing loading effects on the bridge circuitry. High accuracy gains with minimal distortion can therefore be obtained from these high precision instrumentation amplifiers.

The low noise, low gain temperature coefficient, low nonlinearity, and high common mode rejection characteristics of the AD624 amplifier make it ideal for making precise strain measurements with the thin film. The low gain temperature coefficient minimizes thermal effects on the amplifier, while the low nonlinearity reduces high gain amplification distortion. The high common mode rejection of the AD624 amplifier suppresses noise which is common to both amplifier inputs. These factors combine to provide accurate and stable amplification of the thin-film gage output in a high noise environment.

The large gains required to amplify the low-level strain signals require a large gain-bandwith product of the amplifier. Using an amplifier gain of 1000, the 25 MHz gain-bandwidth product of the AD624 amplifier results in a operating bandwidth of 25 kHz.

This is sufficiently wider than the expected useful frequency range (5 kHz) of the thin-film gage.

The low power requirements of the AD624 amplifier, combined with the relatively low voltage (5 V) needed to power the Wheatstone bridge circuit, allow the use of a four (4), 9-V battery, power supply. Therefore, the entire electronics package, including the power supply, is compact and portable. The battery power supply also eliminates grounding problems associated with typical power supplies, and it contributes to the simplicity and ease of use of the amplifier circuit.

The ability to make precise and stable strain measurements on the thin-film gage is greatly dependent on maintaining a constant input voltage to the bridge circuit. Unfortunately, the 9-V power supply is unable to maintain a constant dc voltage across the bridge when loaded by the electronic circuit. For this reason a voltage regulator was needed to stabilize the voltage powering the bridge. The National Semiconductor LM723 voltage regulator was used to provide a stable voltage to the bridge to increase the accuracy and stability of the low-level strain measurements.

High quality, precision components were used to build an electronics package capable of amplifying low-level strain signals in a high noise environment. Proper care must also be taken to shield the entire electronics package, along with the leads, from possible noise sources present in the test environment. Putz [40] offers a review of these noise reduction techniques, along with a complete description of the electronics package developed for the thin-film measurement of skin friction.

Chapter 5

EXPERIMENTAL TESTING OF THE 10X PROTOTYPE

To test the thin-film concept of measuring skin friction, the 10X prototype was statically calibrated and placed in steady and unsteady subsonic flows to measure skin friction. A static calibration of the thin-film prototype was performed to calibrate the output of the thin-film gage when placed in an actual flow. Skin-friction measurements in steady flows were made and compared to Preston tube measurements. The thin-film prototype was also placed in an unsteady flow to measure the unsteady effects of vortex shedding from a cylinder placed in the wind tunnel test section. Survivability testing in a $M = 2.4$ flow was also performed to examine the thin-film gage response in a supersonic environment. These tests were performed to demonstrate the thin-film concept for measuring skin friction and to detect possible design flaws which could be corrected in the final thin-film gage design.

STATIC CALIBRATION OF THE 10X PROTOTYPE

A static calibration of the 10X thin-film prototype allowed the magnitude of the shear force acting on the thin film to be determined when placed in an actual flow. The static calibration also allowed the determination of the thin-film gage sensitivity, output linearity, zero-drift, and hysteresis effects on the gage output under a wide range of simulated shears. Hysteresis effects of the thin film due to frictional effects between the thin film and wall surface were examined by statically loading, then unloading, the thin-film prototype.

A 0.025 mm (0.001 in.) thick 10X prototype gage was attached to the aluminum base plate and each tab was preloaded to 9 N (2 lbs). The two strain gages along one axis of the thin film were wired into a half-bridge configuration of a Wheatstone bridge, as discussed in Chapter 3. The static calibration of the 10X prototype was then performed by hanging weights to a line attached to the center of the active gage surface. A simulated shear force could then be applied to the gage surface along the instrumented axis of the thin-film prototype. The gage was statically loaded in increments of 12 grams to a maximum load of 200 grams. Voltage readings were recorded at each loading increment, then the 10X prototype was unloaded by the same increments. The static loading of the 100 cm^2 (16 $in.^2$) prototype simulated a shear loading on the thin-film gage in increments of 12 N/m^2 (0.0017 $lb/in.^2$) to a maximum shear of 185 N/m^2 (0.027 $lb/in.^2$).

Unfortunately, the thinness of the prototype which allowed an increased sensitivity to strain also resulted in additional problems. The thin-film gage output was dependent on the amount of strain tab preload and to normal forces acting on the gage which result in localized bending of the thin-film surface. Localized bending effects, due to unequal

bending in the strain tabs along each axis of the thin-film gage, resulted in thin-film output not related to the shear levels. Higher preload levels in the tabs resulted in lesser amounts of localized bending in the tabs. Therefore, uniform preload levels along both axes of the prototype were maintained at 22 N (5 lbs) for all testing of the 10X prototype. Localized bending of the thin film resulted in spurious output of the 10X prototype. The half-bridge configuration of the Wheatstone bridge cancels any uniform bending effects on the thin film (i.e., equal bending in both tabs along an axis), but it can not compensate for localized bending effects (i.e., bending in only one tab). Therefore additional strain gages were mounted on the bottom of each strain tab to account for localized bending of the thin-film prototype.

Localized bending effects, in addition to uniform temperature and uniform bending effects, were minimized by mounting four strain gages along each axis of the 10X prototype, as shown in Fig. 12. The Wheatstone bridge was configured in a full-bridge configuration, shown in Fig. 13, which illustrates the placement of the strain gages of Fig. 12. As in the half-bridge configuration, the pair of strain gages on the top surface of the thin-film axis were placed in adjacent arms of the bridge. In addition, the strain gage pair on each tab were placed in opposite arms of the bridge. The full-bridge configuration has the same characteristics as the half-bridge (i.e., uniform bending/ temperature compensation, differential output, and linear output for small resistance changes). In addition, localized bending effects are minimized and the sensitivity of the thin-film gage is doubled because of the additional strain gages. Unfortunately, nonuniform temperature effects which result in unequal thermal output of the strain gages along each axis of the thin film are also doubled.

The output of the full-bridge, E_{out}, can be assumed to be linear and is given by

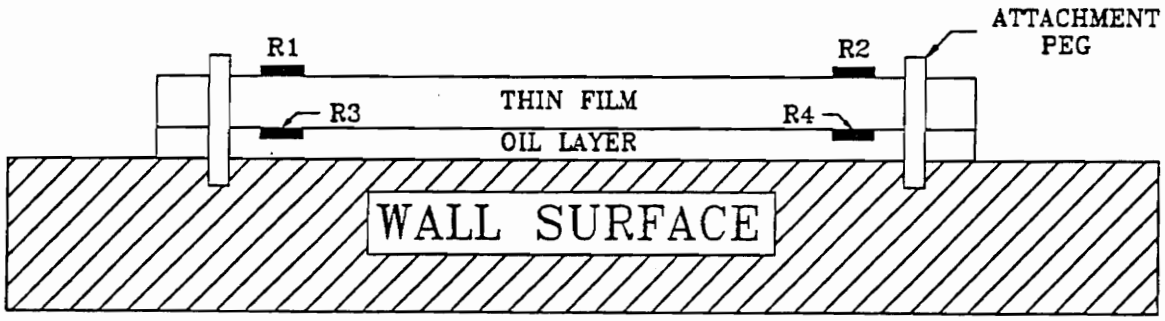

Figure 12. Cross-section of 10X prototype showing mounting of strain gages for localized bending cancellation.

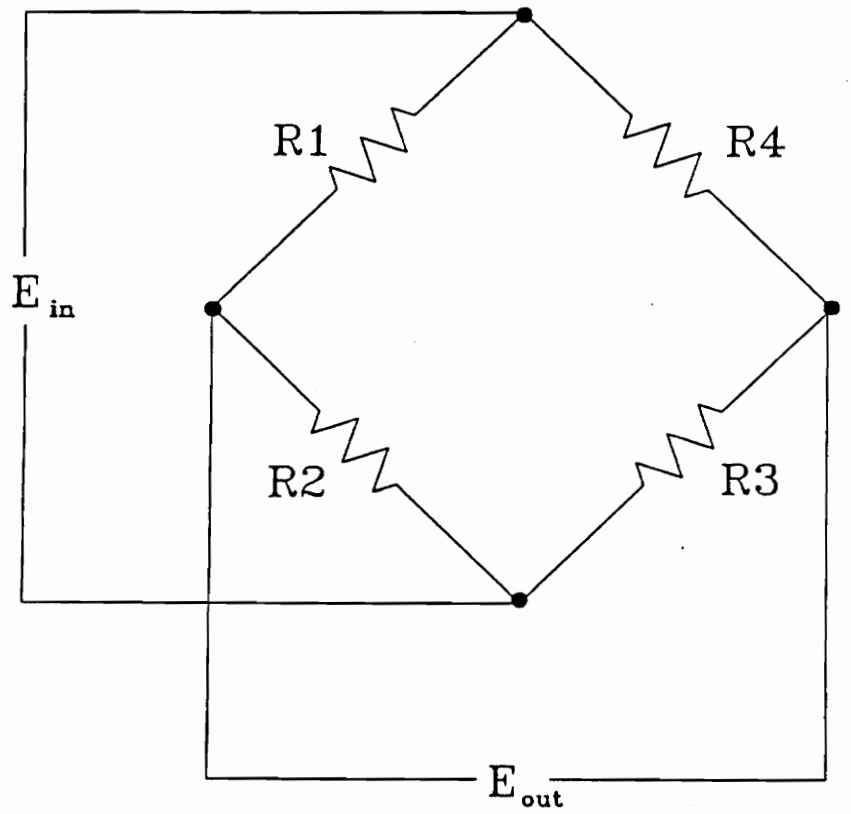

Figure 13. Wheatstone bridge in full-bridge configuration showing placement of strain gages.

$$E_{out} = \frac{E_{in}}{4}\left[\frac{\Delta R_1}{R_1} - \frac{\Delta R_2}{R_2} + \frac{\Delta R_3}{R_3} - \frac{\Delta R_4}{R_4}\right] \qquad [5.1]$$

Shear forces acting on the thin film result in tension forces in one tab, while compressive forces exist in the opposite tab. Assuming tension forces result in positive resistance changes ($\Delta R_1 = \Delta R_3$) , then negative resistance changes occur in the strain gage pair on the opposite tab ($-\Delta R_2 = -\Delta R_4$). Therefore, using Eq. 5.1, the bridge output is given by

$$E_{out} = \frac{E_{in}}{4}\left[\frac{\Delta R_1}{R} - \frac{-\Delta R_2}{R} + \frac{\Delta R_3}{R} - \frac{-\Delta R_4}{R}\right] \qquad [5.1a]$$

where $R = R_1 = R_2 = R_3 = R_4$. This example illustrates the doubling of the thin-film prototype output. Uniform bending/temperature effects are compensated for as in the half-bridge configuration. Localized bending of a single tab results in resistance changes of the opposite sign for strain gages on each tab ($\Delta R_1, -\Delta R_3$). Therefore, assuming only localized bending of one tab, the thin-film gage output predicted by Eq. 5.1 is

$$E_{out} = \frac{E_{in}}{4}\left[\frac{\Delta R_1}{R} + \frac{-\Delta R_3}{R}\right] \qquad [5.1b]$$

where $\Delta R_2 = \Delta R_4 = 0$. Assuming $\Delta R_1 = \Delta R_3$, Eq. 5.1*b* illustrates the cancellation of localized bending effects. Since nonuniform temperature effects result in resistance changes of the same sign for strain gages on the same tab, these effects are doubled.

Static calibrations of the 10X prototype using both half-bridge and full-bridge configurations were performed. The thin-film prototype output was linear and repeatable for both cases as shown in Fig. 14 which compares both the half-bridge and full-bridge calibration curves. The voltage recordings of both calibration curves and the resulting

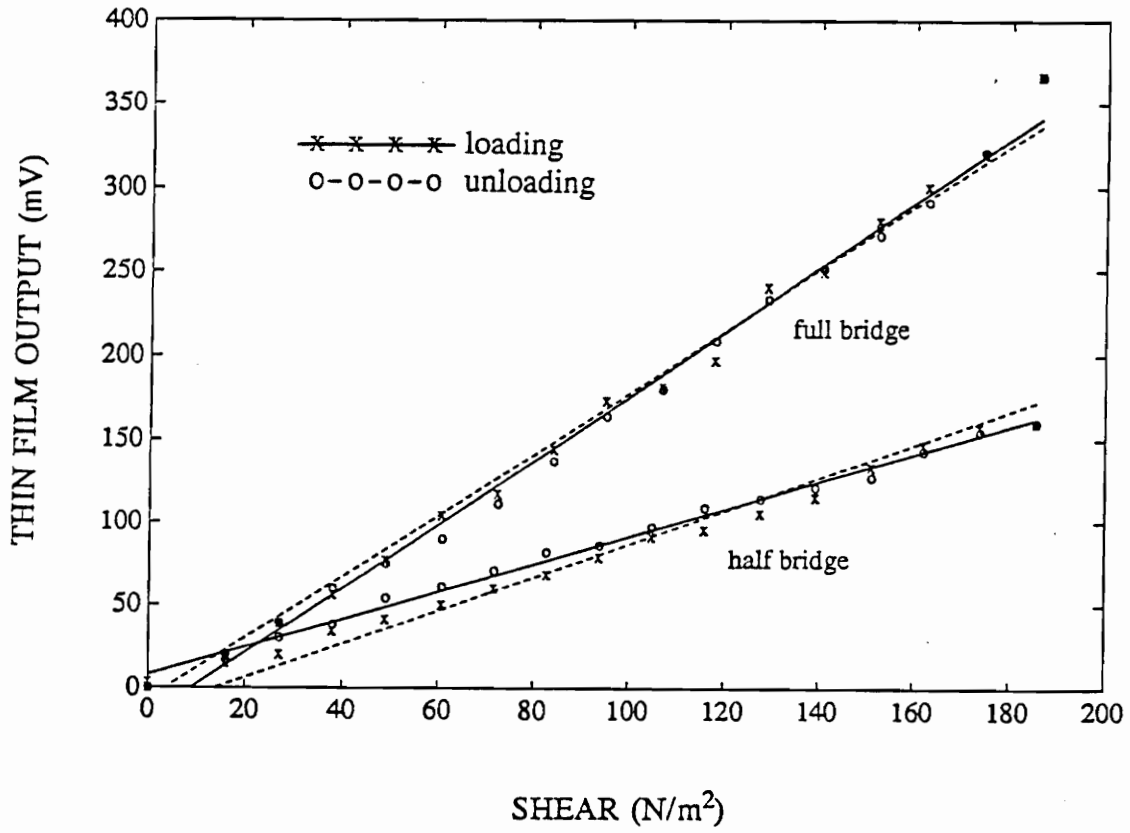

Figure 14. Half-bridge and full-bridge configuration static calibrations of the thin-film prototype.

sensitivities and correlation coefficients, are given in Table 1. The thin-film prototype sensitivity was 0.85 mV/(N/m²) for the half-bridge configuration in loading, and 0.89 mV/(N/m²) in unloading. Likewise, the sensitivities for the full-bridge configuration were 1.9 mV/(N/m²) for both loading and unloading. Thus, the sensitivity was approximately doubled for the full-bridge calibration as expected. The linearity of the thin-film output is demonstrated by the lowest correlation coefficient of 0.985 for all loading cases. Significant zero-drift and hysteresis effects were not observed for the loading range used to calibrate the 10X prototype. The small zero-drift effects are illustrated in Table 1 by the return of the thin-film output to the original zero after being loaded over the entire shear range. Hysteresis effects can be observed by comparing the slopes of the loading and unloading sensitivities for each calibration. A 4% difference in sensitivity slopes for the half-bridge calibration, versus less than 1% for the full-bridge calibration, indicate that the additional strain sensors improve the thin-film output. This effect is thought to be a result of minimizing localized bending effects on the thin film. The output of the prototype was also observed to be sensitive to the line attachment position. This was an expected result of the directional sensitivity of the thin-film gage.

SUBSONIC, STEADY FLOW MEASUREMENTS USING THE 10X PROTOTYPE

Once the static calibration of the 10X prototype was completed, actual skin-friction measurements were made in a steady flow and compared to Preston tube measurements. The entire plate assembly, including the mounted thin-film prototype, was recessed flush

Table 1. Voltage output for half-bridge and full-bridge static calibrations

Shear (N/m^2)	Half-bridge (mV)		Full-bridge (mV)	
	load	unload	load	unload
0.0	0	0	0	0
15.9	20	15	17	19
26.9	30	20	39	39
37.9	38	34	60	56
49.0	54	41	75	77
60.7	61	50	90	104
71.7	71	60	111	117
82.7	82	68	137	144
93.8	86	79	164	173
104.8	97	91	180	181
115.8	109	95	209	197
127.6	114	105	233	240
139.3	121	115	251	249
151.0	127	133	271	279
162.0	143	147	291	300
173.7	155	157	321	320
185.5	160	160	367	367
Sensitivity $mV/(N/m^2)$	0.85	0.89	1.9	1.9
Correlation Coefficient	0.985	0.997	0.997	0.997

to a large wall surface. A Preston tube mounted on a 13 cm diameter aluminum base was also mounted on the wall surface. Both the thin-film prototype and Preston tube were mounted at the same distance from the leading edge of the wall surface as shown in Fig. 15. The wall surface was a 1.8 cm thick painted wood surface (1.2 m x 1.8 m). A rounded leading edge was attached to the wall surface to ensure a smooth boundary layer initiation to the wall surface. A 3.5 cm wide strip of fine sandpaper was attached to the wall surface just behind the leading edge to trip the boundary layer. This trip resulted in a turbulent boundary layer ($Re \cong 1 \times 10^6$) at the gage position, 62 cm downstream of the leading edge.

The wall surface was placed at the exit of a 0.74 m by 0.53 m open-circuit wind tunnel. The flow could be diverted over the wall surface with flaps located at the tunnel exit. Isolating the thin-film prototype by raising the flaps, then lowering the flaps to instantly expose the prototype to the flow, results in step changes in shear forces acting on the thin film. Therefore, the thin-film prototype was operated in an on-off mode. This was necessary to isolate the extremely small shear signal from temperature drift effects in the low velocity flow. Shear measurements were made at flow velocities of 30 m/s (98 ft/s) and 37 m/s (130 ft/s). Other characteristics of the wind tunnel are detailed by Andraka and Diller [42].

Initial tests were performed without an oil layer between the thin film and base plate. Lift-off of the thin film from the plate resulted from air flow underneath the thin film, which also resulted in fluttering of the thin film. Large shear signals, up to a factor of ten greater than expected, resulted from these tests. Shear forces acting on both sides of the thin film and pressure forces acting on the fluttering surface were suspected reasons for the increased readings. To eliminate these problems a thin layer of oil was placed between the thin film and base plate. This oil layer prevented lift-off of the thin

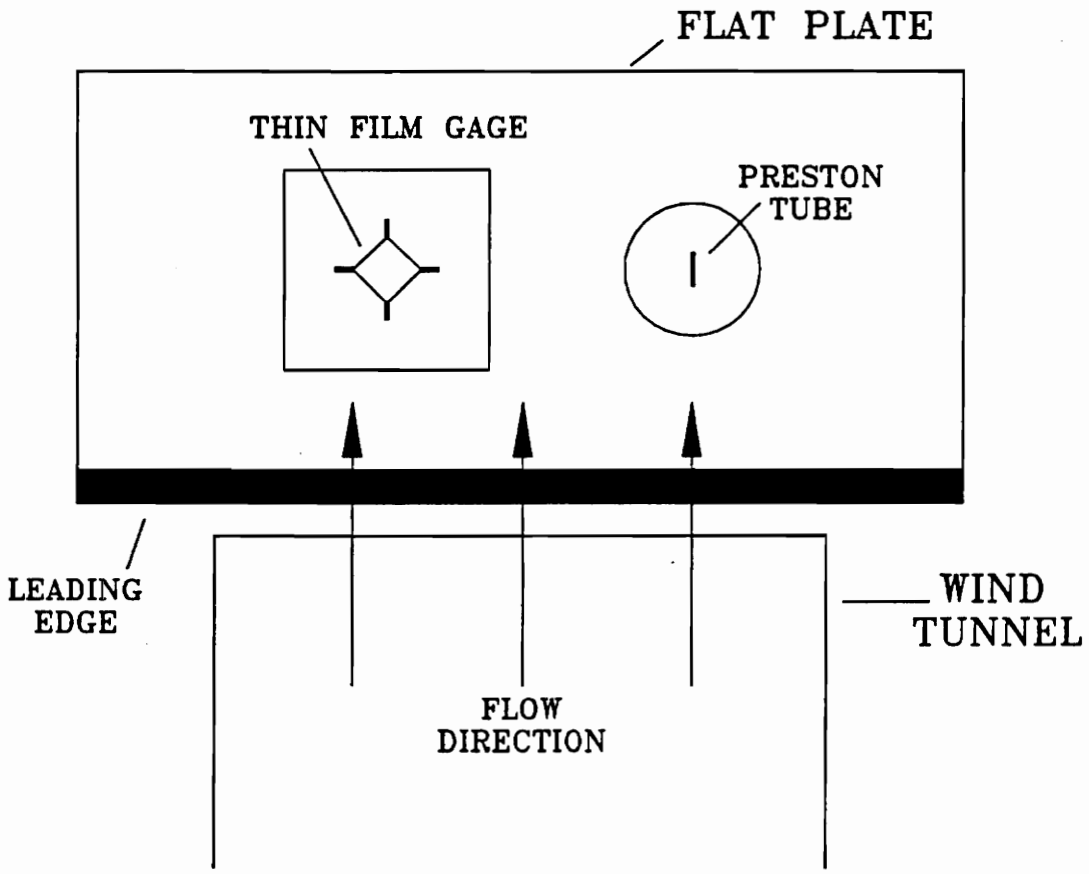

Figure 15. Test apparatus for steady flow calibration of the thin-film prototype.

film, and would also be needed to enhance heat transfer for high temperature measurements.

Skin-friction measurements were made with the thin-film gage at both flow velocities. The entire wall surface/thin-film gage assembly was then rotated 180° to test the directional sensitivity of the thin-film gage. Reversing the flow direction over the thin-film gage should result in output equal in magnitude but of opposite sign. Measurements were made for each flow velocity for both forward and reversed flow. Examples of the thin-film prototype output for each flow velocity and direction are shown in Figs. 16-19. The ability of the thin-film gage to sense flow direction was observed and is shown in the negative step changes in output of Figs. 18-19. Simultaneous Preston tube measurements were also made for each flow condition.

The results of the steady calibration tests are summarized in Fig. 20 on page 57. Shear measurements made in forward flow are shown as positive shear while negative shears indicate measurements made in reversed flow. The thin-film measurement values shown in Fig. 20 are an average of 5 to 10 samples taken for each flow condition. A linear curve fit was used to compare the average thin-film shear measurements to those made with a Preston tube. The calculated skin-friction coefficients obtained from the Preston tube (Patel [8]) averaged $C_f = 0.0032$, which is 14% lower than the frictional coefficient, $C_f = 0.0037$, expected for turbulent flat plate flow (Incropera and DeWitt [43]). An average skin-friction coefficient, $C_f = 0.0044$, was obtained from the thin-film prototype measurements. The skin-friction measurements made with the thin-film gage are approximately 38% higher than the Preston tube measurements.

The extremely low shear levels result in very low signal output of the thin-film prototype. Consequently, the uncertainty in the skin-friction results is large, up to $\pm$ 25% for the thin-film prototype and $\pm$ 5% for the Preston tube (Putz et al. [44]). This uncertainty is illustrated by the fact that the largest shear measured,

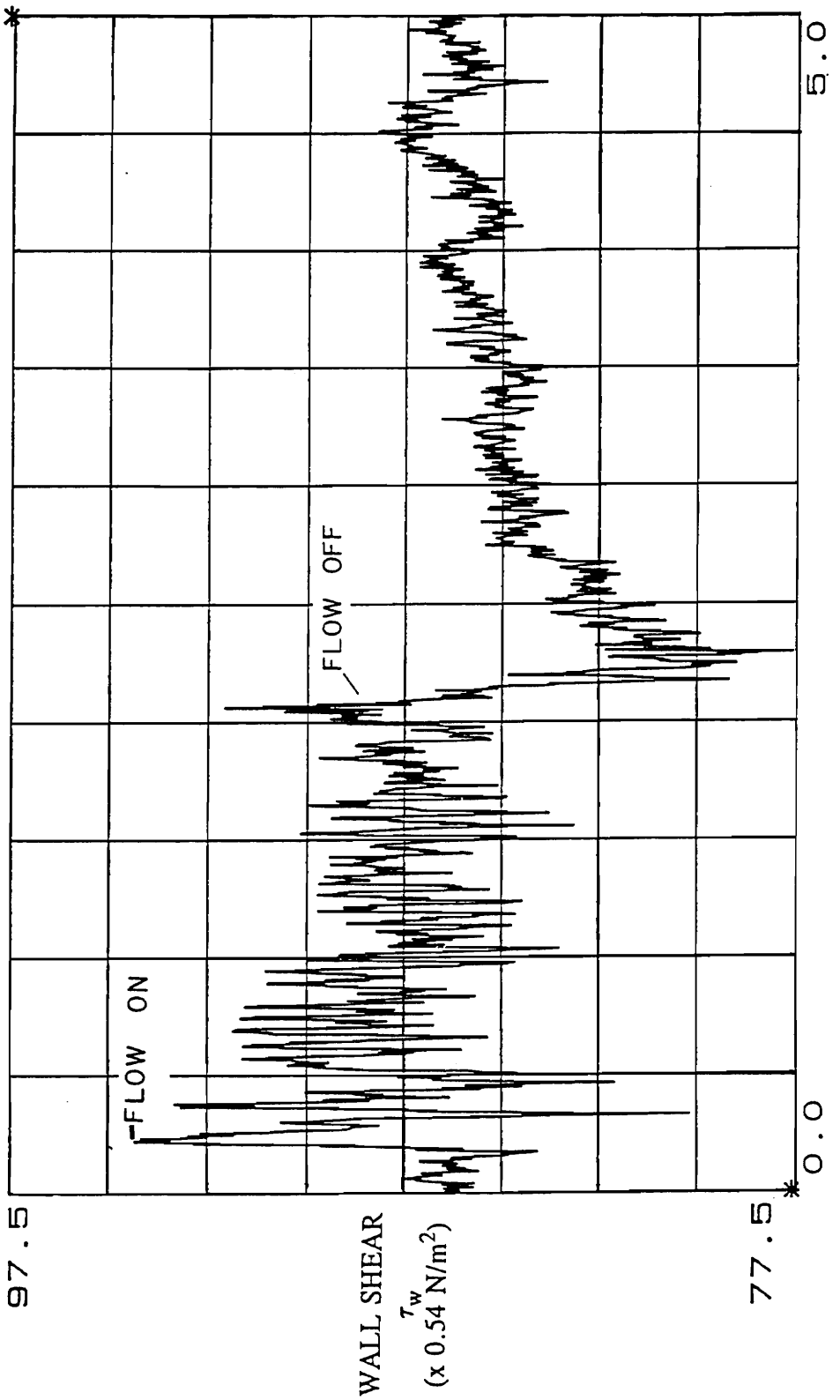

Figure 16. Thin-film gage time signal for forward flow, V = 30 m/s.

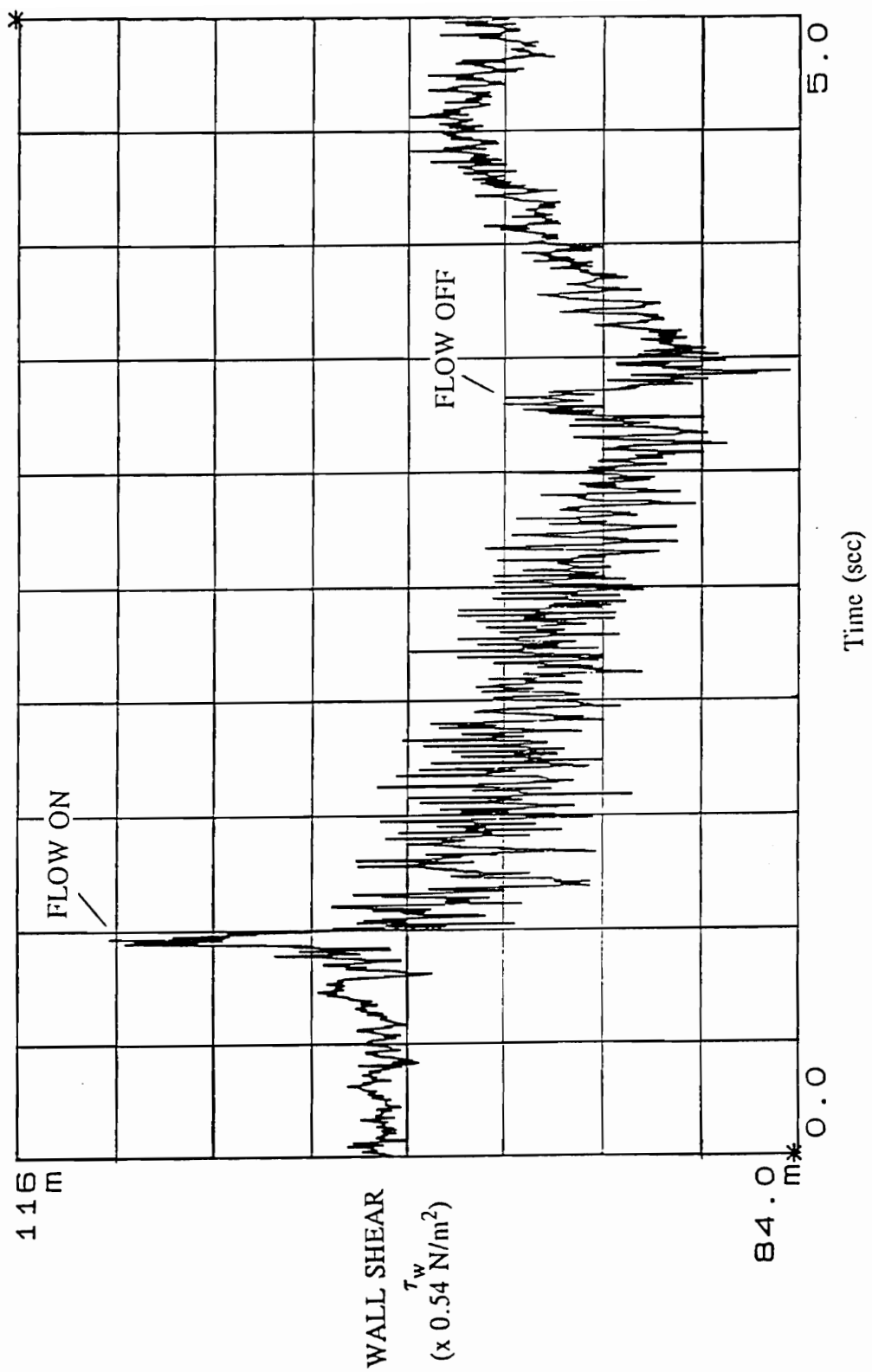

Figure 17. Thin-film gage time signal for forward flow, V = 37 m/s.

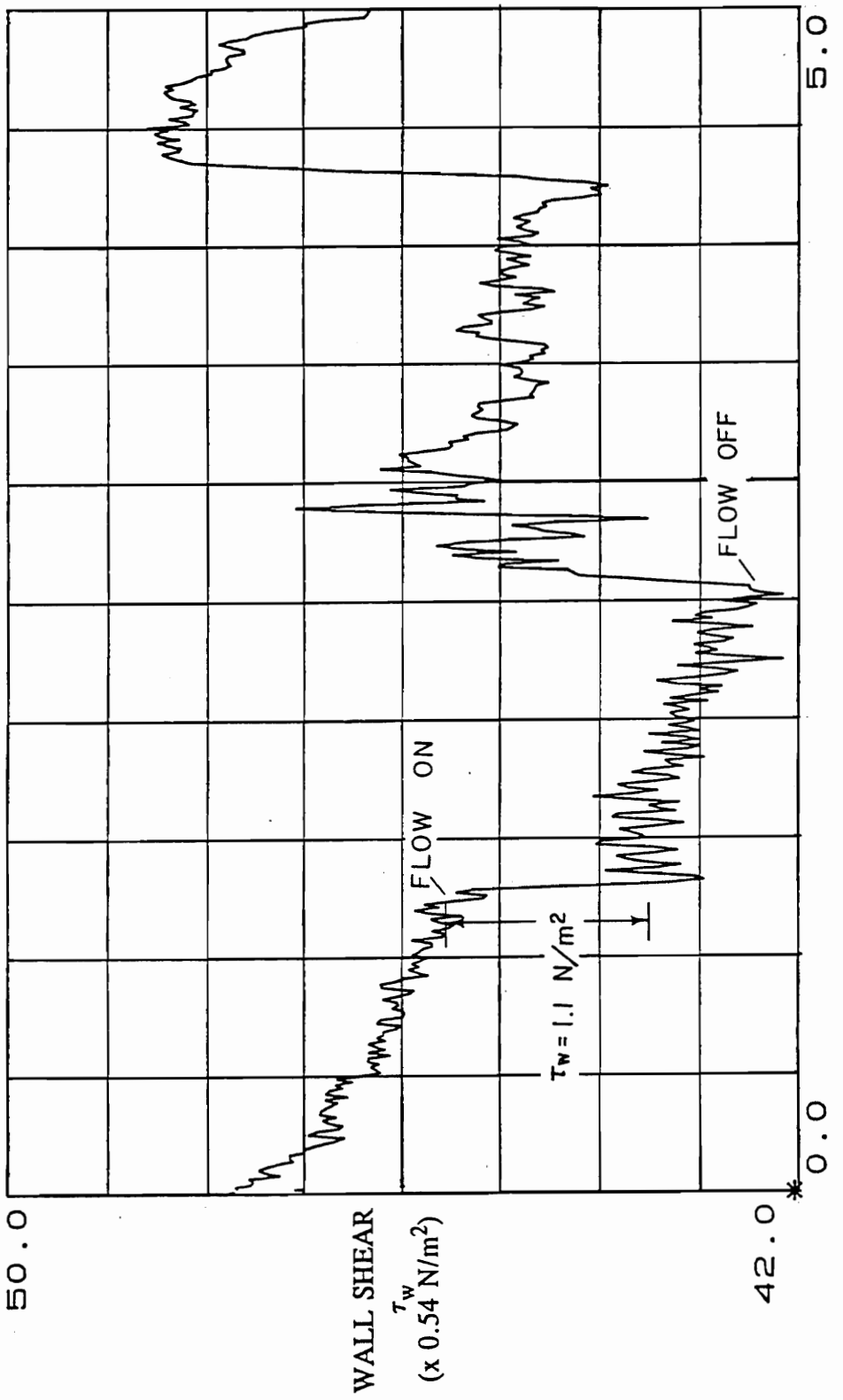

Figure 18. Thin-film gage time signal for reversed flow, V = 30 m/s.

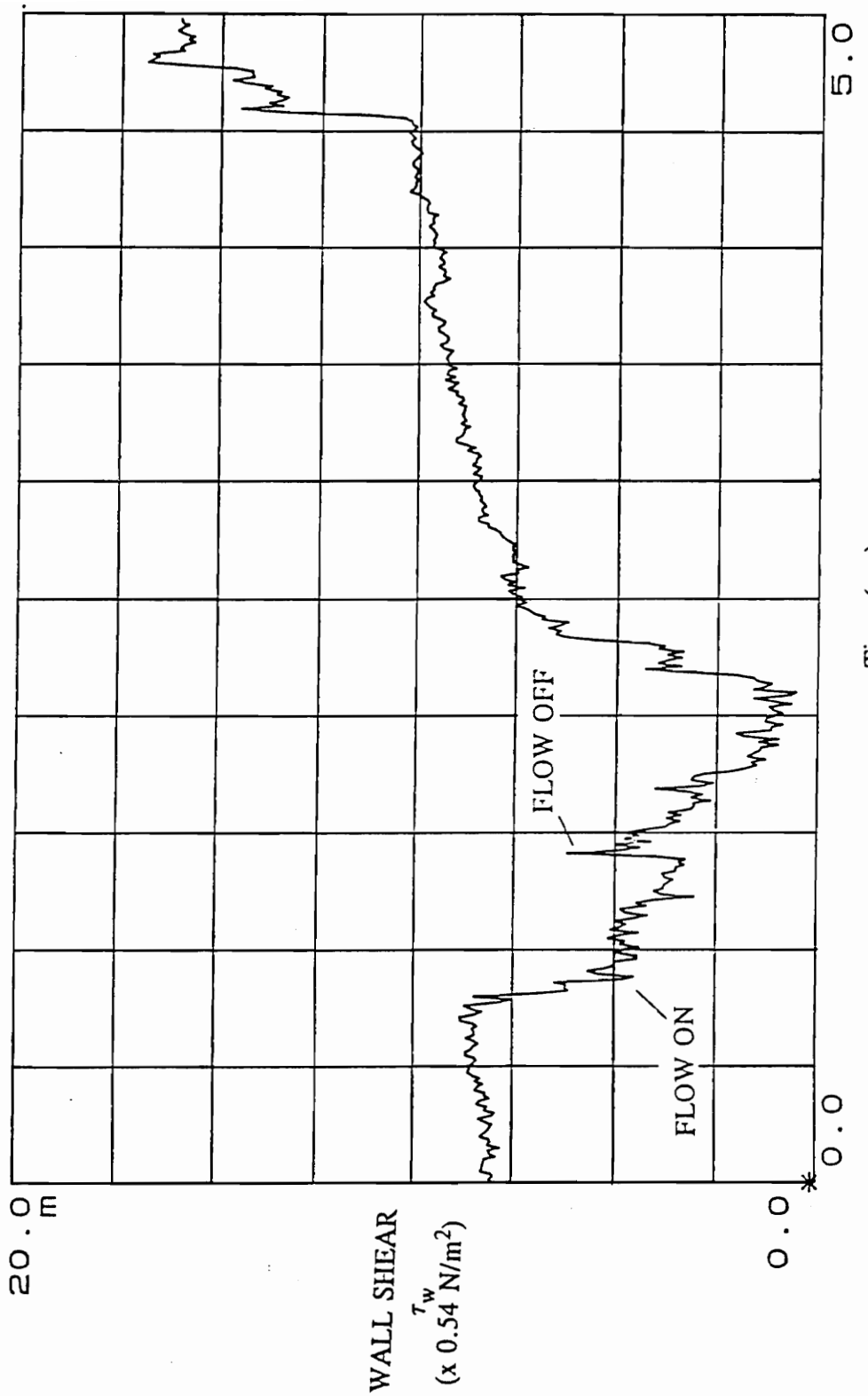

Figure 19. Thin-film gage time signal for reversed flow, V = 37 m/s.

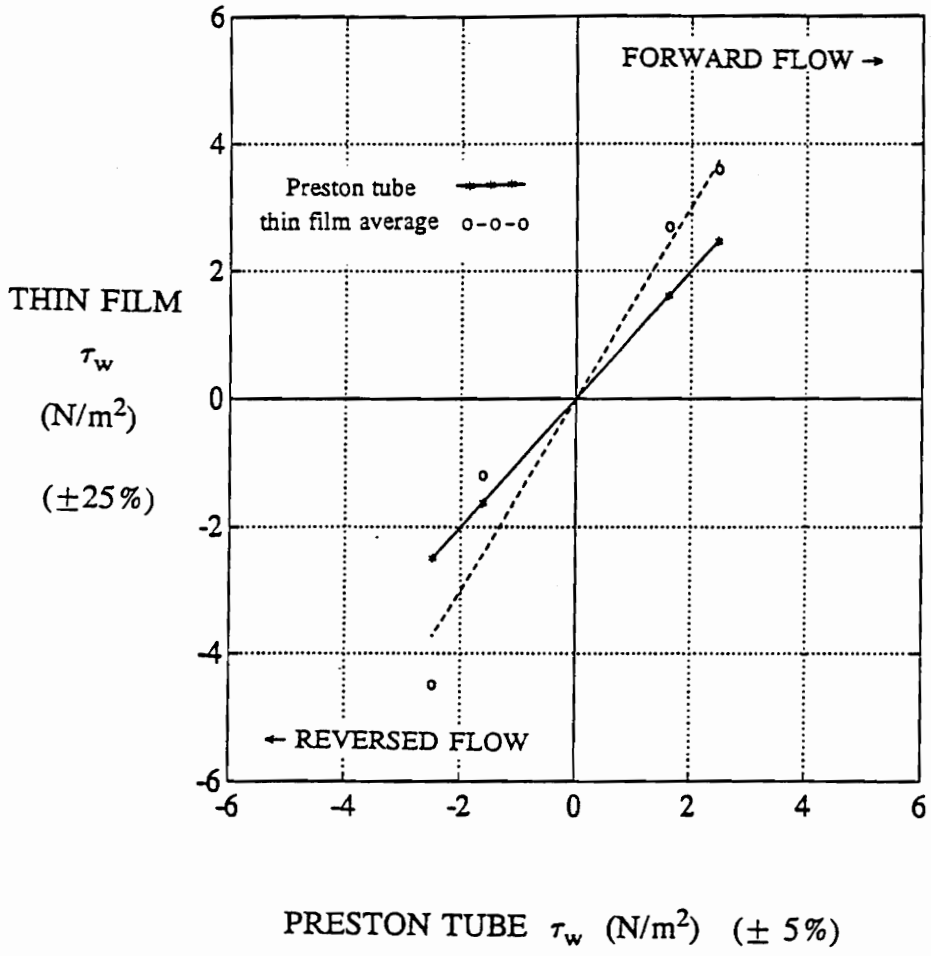

Figure 20. Steady flow testing results comparing 10X prototype measurements to Preston tube measurements.

4 N/m² (0.00056 lb/in.²), is equivalent to a 0.04 N (.009 lb) force acting over the entire 100 cm² (16 in.²) thin-film surface. This shear stress is only a small percentage of the shear stress range over which the thin-film gage was statically calibrated, see Fig. 14 on page 47. The effects of thermal drift also lead to uncertainty in the shear readings. These thermal effects are observed in Figs. 16-19 as the drift of the base output level of the thin-film gage. The 10X prototype was not actively compensated for thermal drift. Later designs of the thin-film gage are planned to compensate for thermal effects by including a thermocouple on each of the strain tabs.

SUBSONIC, UNSTEADY MEASUREMENTS USING THE 10X PROTOTYPE

The 10X prototype can make detailed time-resolved measurements of skin friction because of its high frequency response. The natural frequency of the 10X prototype was calculated as 5 kHz. Therefore, assuming a flat response to 20% of the natural frequency, the useful frequency range is 1 kHz. Skin friction measurements were made in an unsteady flow by mounting the base plate assembly on the floor of a wind tunnel behind a cylinder. The 5 cm diameter cylinder was mounted horizontally midway in the height of the test section. A smaller wind tunnel, of the same design as the tunnel used for the steady flow tests, was used to make measurements at a mean flow velocity of 16 m/s. The tunnel had a test section 0.36 m by 0.25 m, therefore, a 20% blockage of the flow was created by the cylinder. This resulted in a strong vortex shedding signal at 85

Hz. A linearized hot-wire anemometer was mounted just above the thin-film prototype to simultaneously measure the unsteady velocity signal.

An example of the simultaneous velocity and skin-friction measurements obtained from the hot-wire anemometer and thin-film prototype is shown in Fig. 21. This figure illustrates how the thin-film skin-friction signal follows the velocity signal obtained with the hot-wire anemometer. Small fluctuations in skin friction can also be observed in Fig. 21. The ratio of the amplitude of these fluctuations to the peak-to-peak amplitude of the skin-friction signal matches the amplitude ratio obtained from the velocity signal. The magnitude of the skin-friction signal was larger than expected, as compared to the steady flow measurements. This was believed to be due to flow passing under the thin-film gage, a result of not using oil under the thin-film surface. The magnitude of the shear was not the quantity of interest of this test, rather, detection of the unsteady fluctuations in shear with the thin-film prototype. The 85 Hz shedding frequency is clearly shown in the frequency spectrum of the thin-film signal shown in Fig. 22.

SUPERSONIC FLOW TESTING OF THE 10X PROTOTYPE

The response of the thin-film skin-friction gage in a supersonic environment was examined by testing the 10X prototype in a supersonic wind tunnel. Flow conditions were M = 2.4 with a static pressure of 4 psia and total temperature of 300 K. The 10X prototype was mounted on the inside surface of a 34 cm diameter vertical tunnel door.

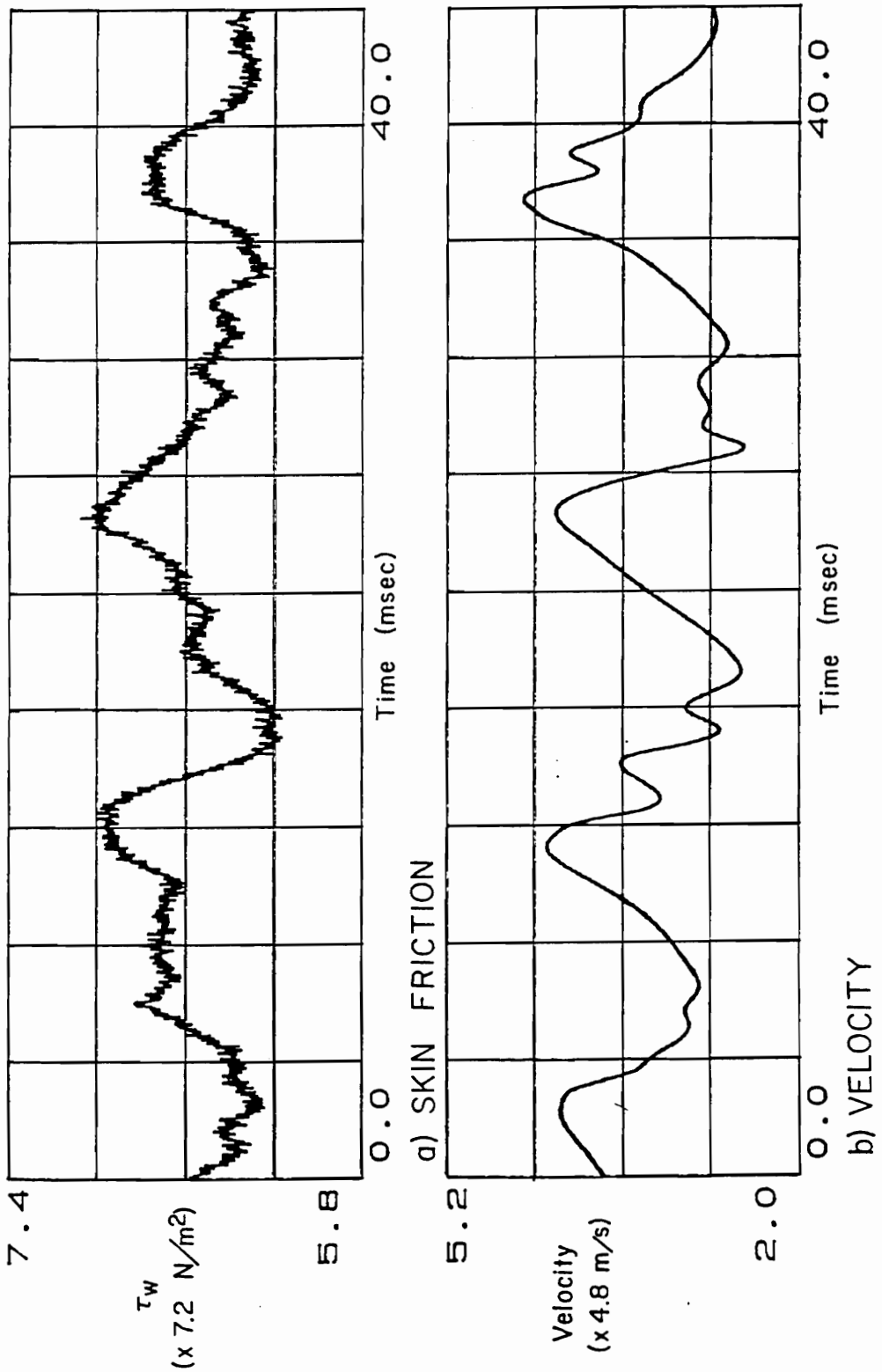

Figure 21. Skin friction and velocity signals in unsteady flow with 85 Hz vortex shedding from a cylinder placed in the flow.

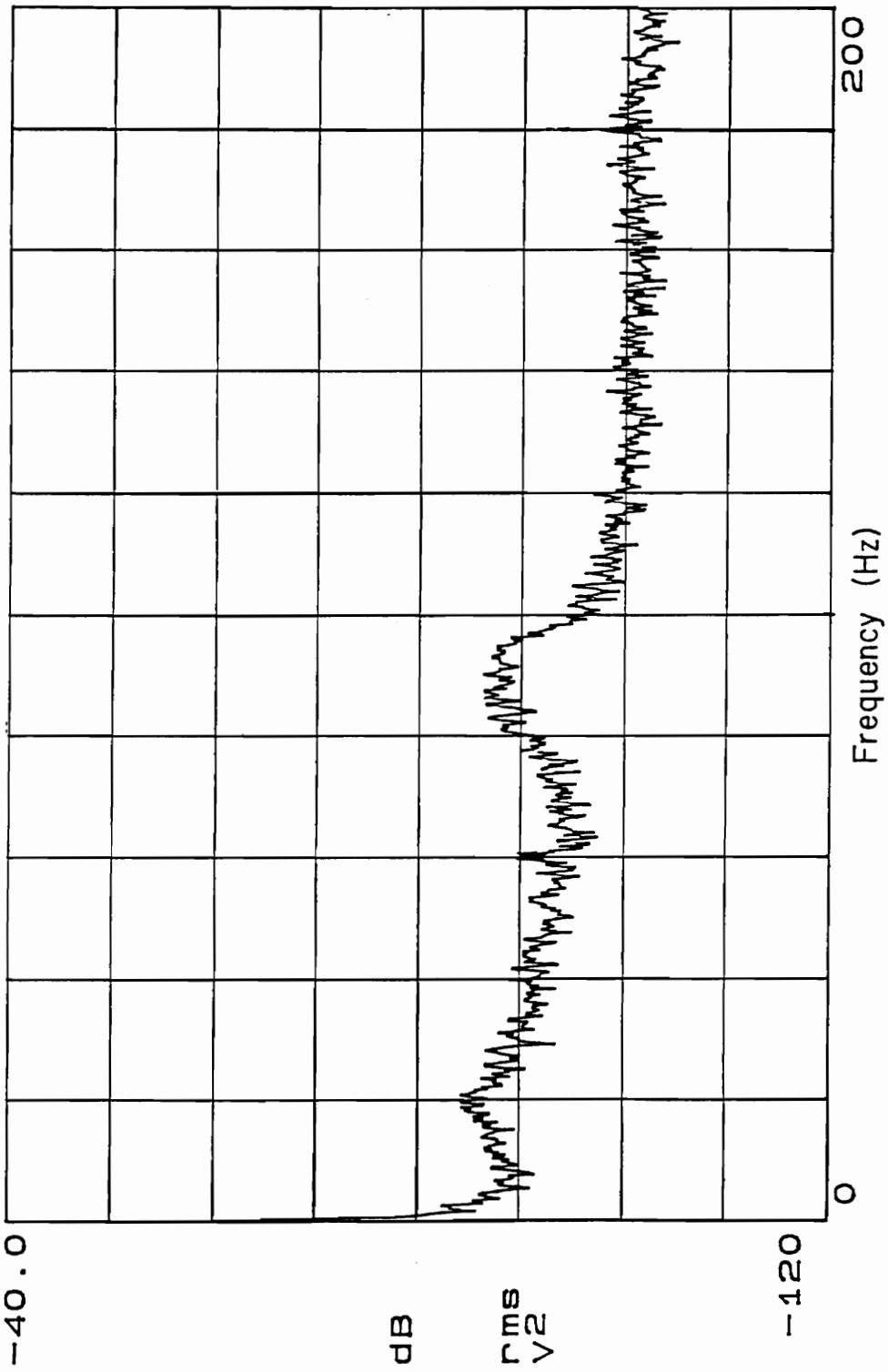

Figure 22. Skin-friction frequency spectrum obtained from thin-film prototype in an unsteady 85 vortex shedding flow.

The inside door surface was flush with the tunnel wall surface to ensure a smooth boundary layer transition.

A 0.13 mm (0.005 in.) thick 10X prototype thin-film gage was mounted flush to the wall surface in a 0.13 mm recess. The prototype was attached to the wall surface with four pins which were mounted in the wall. The pin locations were approximately 0.05 mm greater than the attachment hole locations of the thin film, as described in Chapter 4. Therefore, the thin film had to be heated to fit over the pins which resulted in the desired tension preload in the strain tabs. The attachment tabs were then adhered to the wall surface and the pin heads peened over a small washer used to increase the holding area of the pins. Finally, a thin layer of silicone caulking was placed over the strain and attachment tabs to fill the recess to prevent any flow beneath the thin-film surface.

When the 10X prototype was mounted to the wall surface, it was discovered that the large active surface of the thin film was not flat with the wall. Therefore, a hole through the wall surface and several grooves were machined in the wall surface. A vacuum line was attached to the hole on the back side of the wall surface to pull a vacuum on the back surface of the thin-film gage after oil was placed beneath the thin-film surface. The vacuum line was connected to a 1 liter glass jar which was evacuated with a vacuum pump. The pressure on the back surface of the thin film was maintained at approximately 4 psia. This procedure kept the thin film flat with the wall surface and it also prevented air from becoming entrapped beneath the thin-film surface. Air beneath the thin film would expand during tunnel blow-down which could cause lifting and failure of the thin-film gage.

Several 0.13 mm 10X prototypes failed to survive the supersonic flow conditions. A high-speed camera used to film the thin-film response showed that flow penetrated beneath the leading edge of the thin film. This caused the thin film to lift from the wall surface and begin to flutter in the flow, eventually leading to its failure.

To correct the problems associated with flow beneath the gage, a 0.25 mm (0.010 in.) thick 10X prototype was recessed and mounted approximately 0.2 mm beneath the wall surface. A thicker gage was used because of the concern of the flutter-mode failure observed with the 0.13 mm thin-film prototype. The same mounting procedure was used as previously discussed, and a vacuum was pulled on the back side of the thin film to keep it flat. The 0.25 mm thin film survived the supersonic blow-down. The same thin-film prototype was then instrumented with strain gages to make shear measurements. The strain tabs on the instrumented prototype could not be covered with silicone, however, which resulted in the entire gage surface not being as flat as in the survivability test. Unfortunately, this led to the failure of the 0.25 mm prototype during blow-down.

Although several failures of the 10X prototype occurred during the supersonic testing, several things were learned during these tests. Recessing the thin film beneath the wall surface and removing any air pockets from beneath the thin-film surface aided in the survivability of the thin film. Also, concerns over methods of attachment and flutter-mode failure were raised. Fluttering of the thin film indicated that the thin film was not rigid enough to withstand vibrations induced by the supersonic flow. This effect could be eliminated by using a thicker film to construct the gage, but this would also lead to reduced sensitivity of the gage. The difficulty encountered in attaching the thin film to the wall also had to be addressed before a smaller version of the thin-film gage could be constructed.

Difficulty in keeping the thin-film surface flat was a major obstacle which required the need for pulling a vacuum on the backside of the thin-film surface. These surface distortion problems encountered with the 10X prototype may not be as significant for future designs of a 1 cm by 1 cm gage. The reduced scale of the thin film increases the relative stiffness of the thin film which is critical to the survivability of the thin film in

a supersonic environment. The identification of these problems through supersonic testing of the 10X prototype was helpful in designing an actual-size (1X) prototype thin-film gage for use in a supersonic environment.

SUMMARY

Calibration and testing of the 10X prototype for both subsonic and supersonic measurements of skin friction provided a great deal of information about the performance of the thin-film gage. The static calibration of the 10X prototype demonstrated that hysteresis effects resulting from friction between the thin-film and wall surface were small. Significant frictional effects could have greatly reduced the ability of the thin-film gage to accurately measure skin friction. The thinness of the 10X prototype (0.001 in.) caused problems in attachment of the thin film to the wall surface and maintaining a flat thin-film surface. This required the mounting of additional strain gages and pulling a vacuum on the back surface of the 10X prototype gage. Increasing the stiffness of the 1X prototype, by reducing the size of the prototype while maintaining the same thickness (0.001 in.), eliminated these problems associated with the 10X prototype. Finally, the layer of oil between the thin-film and wall surface greatly improved the 10X prototype performance. The oil layer effectively prevented air flow beneath the thin-film surface, maintained the thin-film flat with the wall surface, and acted as a fluid damper to any vibration of the thin-film surface caused by the flow.

Chapter 6

DEVELOPMENT AND EXPERIMENTAL TESTING OF A 1X THIN-FILM PROTOTYPE

The fabrication and experimental testing of the 10X prototype provided useful information for the design of an actual-size (1X) prototype of the thin-film gage. Problems associated with attachment of the thin film to the wall surface and the need for a relatively rigid thin-film surface were considered in the design of the 1X prototype. A 1 cm by 1 cm thin-film gage was fabricated and instrumented with commercially available semiconductor strain gages. The thin-film gage was then mounted to a probe head which served as the wall surface. The 1X prototype was then statically calibrated to make skin-friction measurements in subsonic and supersonic flows.

FABRICATION OF THE 1X PROTOTYPE

Attachment and alignment problems encountered in mounting the 10X prototype were eliminated by modifying the pattern of the thin-film gage. Intead of cutting the thin-film gage (i. e., active surface, strain tabs, and attachment tabs) from the shim stock and attaching it to the wall surface, the active surface and strain tab elements were only partially cut from the shim stock. The surrounding material was left to give a much larger attachment surface which is farther from the active element. The new thin-film pattern, shown in Fig. 23, eliminates the problem of the tab attachments. In addition, the attachment surface keeps the axes of the thin film orthogonal to each other.

A 1X prototype thin-film gage was cut from 0.05 mm (0.002 in.) stainless steel shim stock. A laser was used to accurately cut the thin slits (0.025 mm) in the thin film. The outside diameter of the attachment surface was cut to 3.5 cm (1.375 in.) to fit on a probe head which served as the wall surface. Commercially available strain gages were mounted on the strain tabs. The extremely small strain gages (0.23 mm by 2 mm) fit easily on the strain tabs. Semiconductor strain gages (Micro Gage Inc., #919-P-1000-04) were used because of their small size and large gage factor of 170. The large gage factor gives an increased sensitivity of the thin-film gage. Unfortunately, the semiconductor strain gages are also more sensitive to temperature effects than metal-foil strain gages.

The 1X prototype thin-film gage was mounted on a stainless steel probe head, see Fig. 24. A two-part epoxy was used to adhere the thin film to the probe head. The thin-film gage was mounted with the strain gages between the thin-film surface and probe head. Therefore, the strain sensors were isolated from the flow which offers several advantages. The strain gages and leads are protected from the potentially harmful flow and convective effects are reduced. Also, the leads can be run out of holes in the

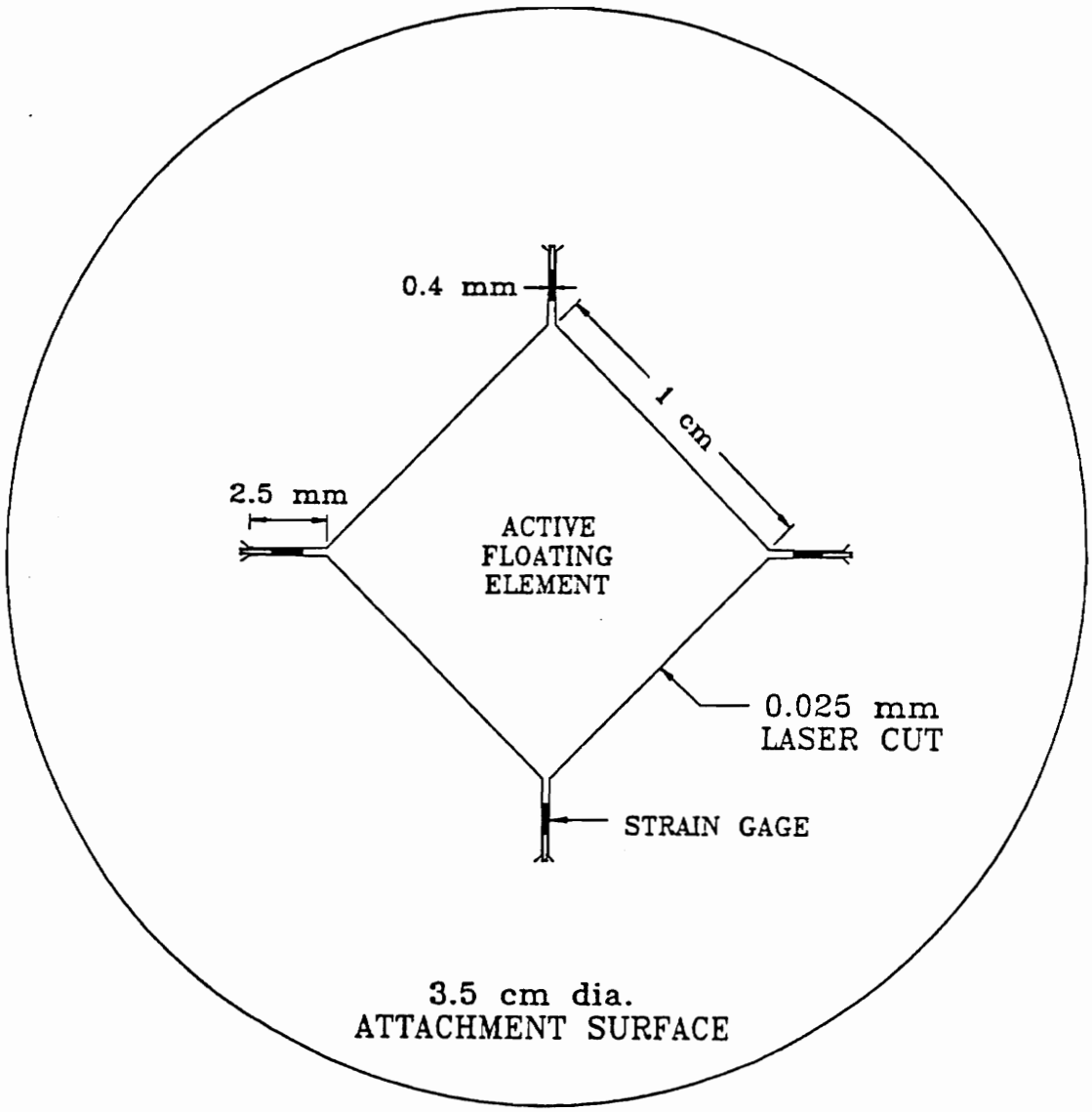

Figure 23. Actual-size (1X) prototype of the thin-film shear stress gage.

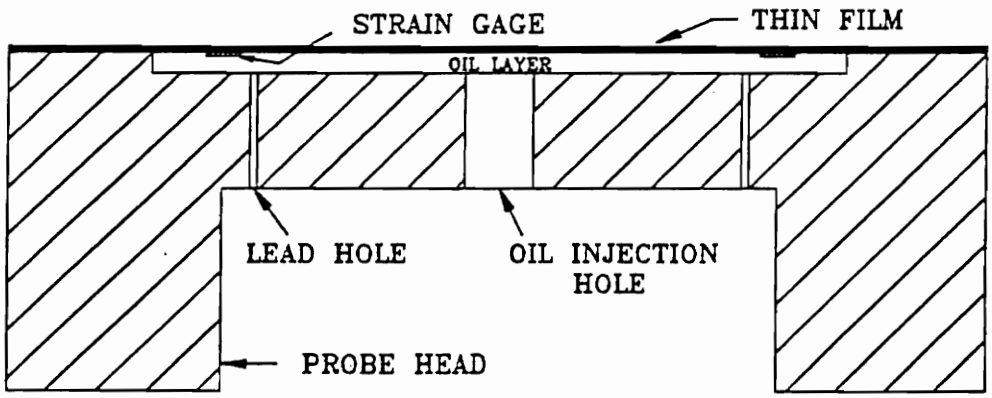

Figure 24. Mounting of the 1X prototype to the probe head.

backside of the probe head. Oil was injected into a 0.13 mm (0.005 in.) recess beneath the gage through a hole in the backside of the probe head. The lead and oil injection holes were sealed and the entire thin film/probe head assembly was placed in an evacuated chamber to draw any air from beneath the thin-film surface. The strain gages along each axis of the thin-film gage were wired into a half-bridge configuration of a Wheatstone bridge which was part of the electronics package used to amplify the output of the 10X thin-film prototype, as discussed in detail in Chapters 3 & 4.

SUPERSONIC TESTING OF THE 1X PROTOTYPE

After fabrication and mounting of the 1X prototype was completed, supersonic flow tests of the thin-film prototype were performed. Supersonic testing was performed before subsonic testing because it was critical to demonstrate the survivability of the thin-film gage in a supersonic environment. Once the thin-film survivability tests were completed, the 1X prototype was instrumented to make actual skin-friction measurements. These results could then be compared to skin-friction measurements made with a floating element balance (DeTurris et al. [38]).

The first thin-film prototype tested did not have an oil layer beneath the thin-film surface. This was done to observe the effect of a fluid layer on the behavior of the thin-film surface during supersonic flow testing. The thin-film prototype survived the initial start-up transients and steady periods of the supersonic tunnel blow-down. Vibration of the active surface was observed during the test, especially during the start-up transients. The attachment of the thin film to the probe head failed during the tunnel shut-down, a period when the static pressure fluctuates significantly. The pressure dif-

ferential across the thin-film surface caused it to bow outward into the flow, and led to the ultimate failure of the thin-film attachment. The failure was caused by the failure of the epoxy adhesive used to attach the thin-film to the wall surface.

A second 1X prototype, with oil beneath the thin-film surface, was tested in a supersonic flow to determine the effect of the oil layer on the thin-film surface during blow-down. The oil damped out the majority of the thin-film surface vibrations caused by the supersonic flow. Vibration of the active surface was observed only during tunnel start-up and shut-down, periods of high flow unsteadiness. The gage survived several supersonic blow-downs. Several other 1X prototypes with oil beneath the active surface were tested in an extended blow-down. The relatively long run time, approximately one minute, resulted in subsonic flow through the test section at the time of shut-down. This reduced the severity of the pressure differential across the thin-film surface, and resulted in the successful survival of the thin-film prototype. Vibration of the active surface was observed while the flow was sonic as shock waves passed over the thin-film surface. The majority of the thin-film gages failed during relatively short blow-downs of approximately five seconds. The large pressure differentials which resulted during shut-down caused the failure of the thin-film attachment to the probe head.

The need to improve the thin-film attachment to the probe head was demonstrated by the previously discussed testing. To eliminate the attachment problems the thin-film surface was spot-welded to the probe head instead of using an epoxy adhesive. Approximately fifty (50) individual spot-welds were made on the perimeter of the thin-film attachment surface. The low voltage required to weld the thin-film surface to the probe head resulted in virtually no heating, distortion, or thermal stresses developing in the thin-film surface. The edge of the attachment surface was then sanded to smooth the surface, and a thin layer of epoxy was applied along the edge of the attachment surface to seal the thin-film surface.

Several 1X prototypes, with the spot-welded attachment and oil beneath the thin-film surface, were tested in a supersonic flow. All of the thin-film prototypes survived the supersonic blow-down. Both long and short blow-downs were performed to test the thin-film attachment. Again vibration of the active surface was observed as shock waves passed over the thin-film surface. Problems associated with this vibration during start-up and shut-down of the supersonic tunnel may have to be addressed in future testing. These survivabilty tests demonstrated that the thin-film skin-friction gage could survive a supersonic environment.

STATIC CALIBRATION OF THE 1X PROTOTYPE

The 1X prototoype was statically calibrated to determine the magnitude of the shear forces acting on the thin film when placed in subsonic and supersonic flows. The static calibration allowed the sensitivity and linearity of the thin-film gage output to be determined. The calibration was performed by hanging weights to a line attached to the center of the active surface. The thin-film gage was loaded in increments of 1 gram to a maximum load of approximately 17 grams. The voltage output of the thin-film prototype was recorded at each loading increment. The static loading of the 1 cm^2 prototype simulated a shear loading in increments of 100 N/m^2 (0.015 $lb/in.^2$) to a maximum shear of 1650 N/m^2 (0.24 $lb/in.^2$). The 1X prototype was not unloaded, as in the 10X static calibration, because of the difficulty in unloading the thin-film gage. The small weights used to calibrate the 1X prototype could not be unloaded without significantly disturbing the system.

Several static calibrations of the 1X prototype were performed. The thin-film prototype was calibrated twice with a unity gain (G = 1) set on the amplifier. This was done to test the repeatability of the thin-film gage output. The 1X prototype was also calibrated with an approximate amplifier gain of 100 (G ≅ 100). This was done to amplify the signal to a convenient level. The voltage recordings obtained from the static calibrations, and the resulting sensitivities and correlation coefficients, are given in Table 2. The output obtained from the unity gain calibrations was linear and repeatable as illustrated in Fig. 25. The resulting sensitivities were 0.0025 mV/(N/m²) and 0.0021 mV/(N/m²). Figure 26 shows the static calibration results obtained using an amplifier gain of approximately 100. The sensitivity obtained from this calibration was .32 mV/(N/m²). The linearity of the calibration curves is demonstrated by the lowest correlation coefficient of 0.992 for all calibrations of the 1X prototype.

Table 2. Voltage output of 1X thin-film prototype static calibration.

Shear	Voltage Output (mV)		
(N/m^2)	G = 1	G = 1	G ≅ 100
0	0.0	0.0	0
49	0.2	-0.3	10
127	0.2	0.2	50
224	0.4	0.3	100
318	0.5	0.5	130
410	0.6	0.8	140
505	0.7	0.9	170
603	1.2	0.8	200
712	1.6	1.3	230
808	1.7	1.5	260
896	2.2	1.8	290
993	2.4	1.9	320
1106	2.6	2.2	360
1185	2.7	2.5	390
1275	3.3	2.7	410
1364	3.2	2.8	440
1454	3.4	3.0	460
1568	3.7	3.3	510
1646	3.9	3.4	530
Sensitivity $mV/(N/m^2)$	0.0025	0.0021	0.32
Correlation Coefficient	0.992	0.995	0.999

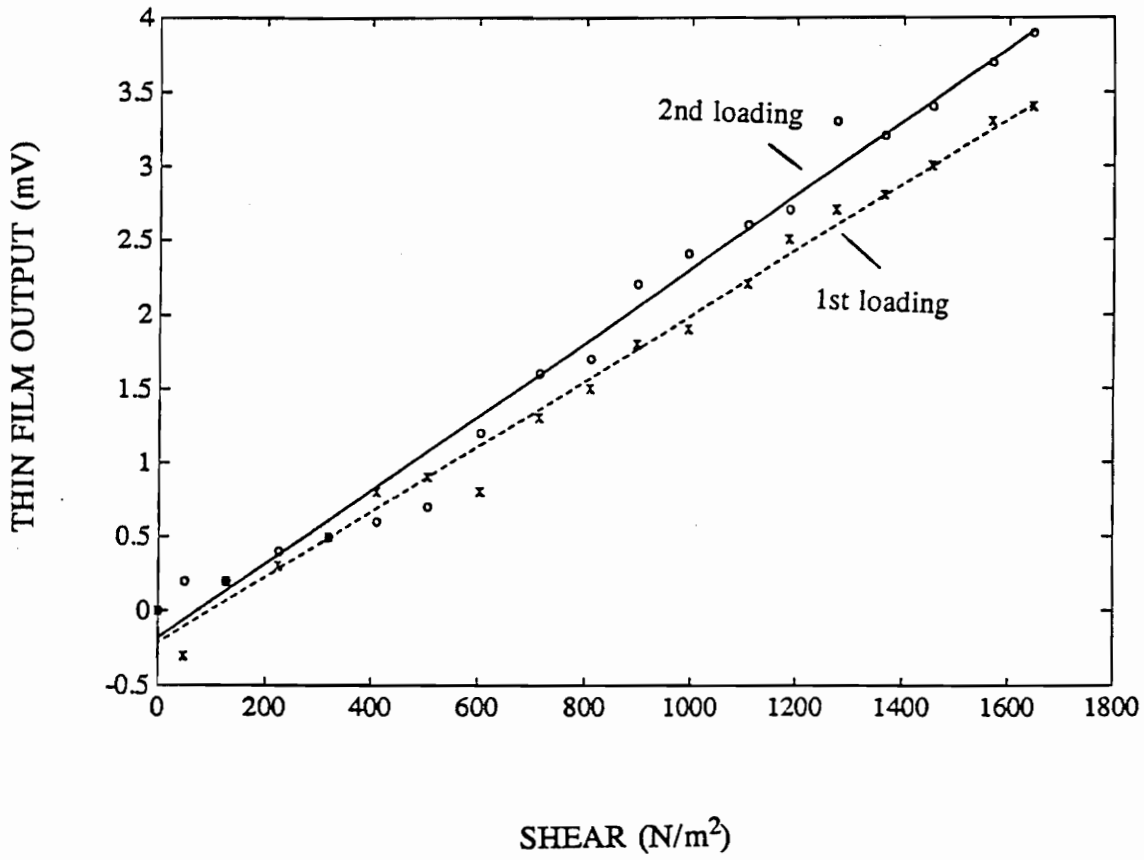

Figure 25. Static calibration of 1X prototpye with unity gain amplification.

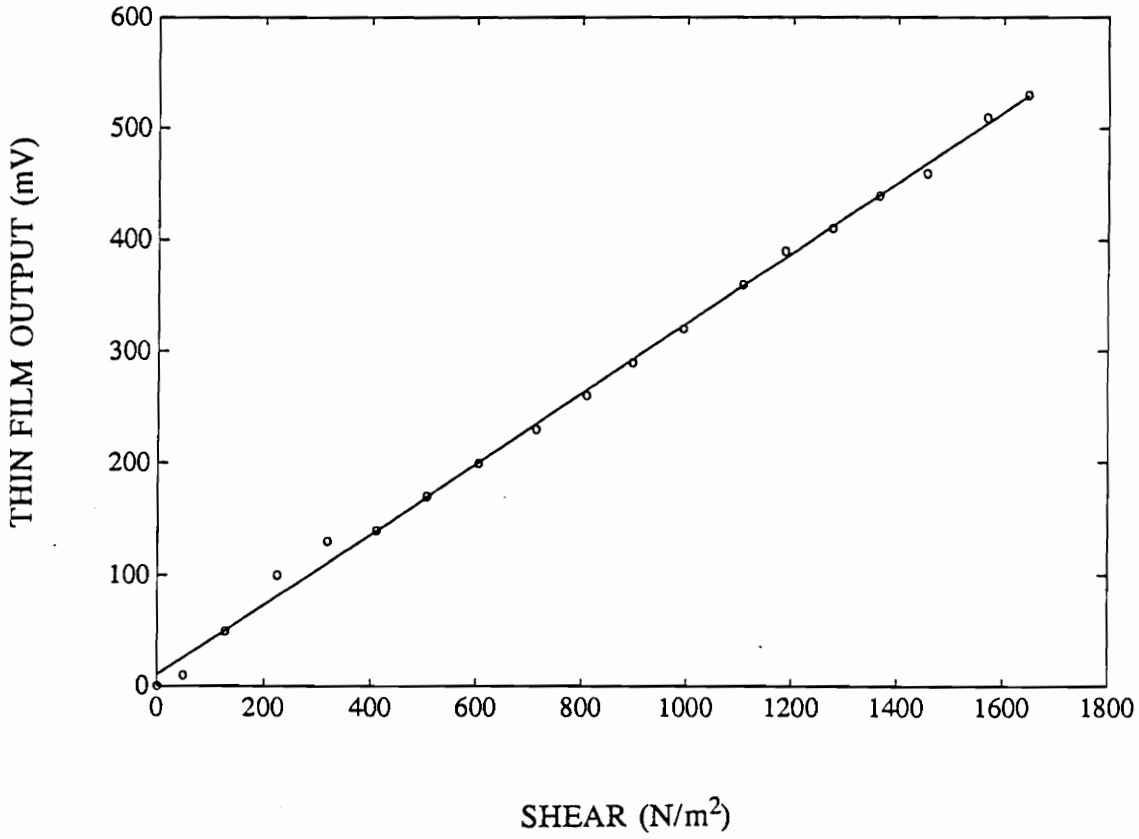

Figure 26. Static calibration of 1X prototype with approximately 100X amplification.

Chapter 7

CONCLUSIONS AND RECOMMENDATIONS

CONCLUSIONS

The purpose of this research was to develop and perform initial testing on a direct-force-reading, thin-film shear stress gage. The following conclusions were drawn from the research.

- The advancements made during the research and the potential improvements to existing skin-friction measurement technology justify continued development of the thin-film shear stress gage.

- Calibration and initial testing of a large-scale (10X) prototype have demonstrated the thin-film concept for measuring skin friction as verified by,

- the linearity and repeatability of the calibration curve obtained from a static calibration of the thin-film prototype

- the directional sensitivity and the extremely small shears measured with the thin-film prototype during steady flow tests

- the high frequency response of the thin-film gage for time-resolved measurements of skin friction in unsteady flows.

- Temperature effects on strain measurements were observed to be a significant problem during testing of the 10X prototype. Compensation for these thermal effects can be performed by monitoring the temperature of each strain tab with thermocouples.

- Concern over the relative stiffness of the thin-film gage was raised during supersonic testing of the 10X prototype. A trade-off between stiffness and sensitivity results from increasing the thickness of the thin-film gage.

- Development of an actual-size (1X) prototype, with the redesigned thin-film pattern, eliminated attachment and alignment problems associated with the original thin-film design. Laser cutting the active surface and strain tabs from a larger thin-film surface led to the following improvements,

  - providing a greatly increased attachment area for improved attachment of the thin-film gage to the wall surface

  - elimination of problems associated with alignment and preload uniformity of the strain tabs during attachment of the thin-film gage to the wall surface.

- Testing of the 1X prototpye in a supersonic flow demonstrated that the thin-film gage could survive a supersonic environment.

- Considerable development of the thin-film gage is required to attain a gage suitable for testing in a scramjet environment.

RECOMMENDATIONS

The following recommendations are made for future development of the thin-film shear stress gage.

- Obtain initial skin-friction measurements with the 1X prototype in supersonic flow. This is critical to demonstrate the ability of the thin-film gage to accurately measure skin friction in a supersonic environment.

- Begin to make thermally compensated skin-friction measurements with the 1X prototype in subsonic and supersonic flows.

- Perform steady flow calibration of the 1X prototype with existing skin-friction measurement devices (i. e., Preston tube and floating element balance).

- Begin microfabrication (sputtering) of strain sensors directly onto the thin-film surface for high temperature strain measurement.

REFERENCES

1. Kempf, G. (1929) "Neue Ergebnisse der Widerstandsforschung," Werft, Reederei, Hafen 11, pp. 234-239.

2. Schoenherr, K. E. (1932) "Resistance of flat surfaces moving through a fluid," Trans. Soc. nav. Archit mar Engrs., New York, Vol. 40, pp. 279-313.

3. Brown, K. C., and Joubert, P. N. (1969) "The Measurement of Skin Friction in Turbulent Boundary Layers with Adverse Pressure Gradients," Journal of Fluid Mechanics, Vol. 35, part 4, pp. 737-757.

4. Winter, K. G. (1977) "An Outline of the Techniques Available for the Measurement of Skin Friction in Turbulent Boundary Layers," Prog. Aerospace Sci., Vol. 18, pp. 1-57.

5. Clauser, F. H. (1954) "Turbulent Boundary Layers in Adverse Pressure Gradients," Journ. Aeronaut. Sci., Vol. 21, pp. 91-108.

6. Preston, J. H. (1954) "The Determination of Turbulent Skin Friction By Means of Pitot Tubes," Journ. Roy. Aeronaut. Soc., Vol. 58, pp. 109-121.

7. McAllister, J. E., Pierce, F. J., and Tennant, M. H. (1982) "Preston Tube Calibrations and Direct Force Floating Element Measurement in a Two-Dimensional Turbulent Boundary Layer," Journal of Fluids Engineering, Vol. 104, pp. 156-160.

8. Patel, V. C. (1965) "Calibration of the Preston Tube and Limitations on Its Use in Pressure Gradients," Journal of Fluid Mechanics, Vol. 23, part 1, pp. 185-208.

9. Frei, D., and Thomann, H. (1980) "Direct Measurements fo Skin Friction in a Turbulent Boundary Layer with a Strong Adverse Pressure Gradient," Journal of Fluid Mechanics, Vol. 101, part 1, pp. 79-95.

10. Nitsche, W., Haberland, C., and Thunker, R. (1984) "Comparative Investigations on Friction Drag Measuring Techniques in Experimental Aerodynamics," ICAS-84-2.4.1, 14th Congress of the International Council of the Aeronautical Sciences, pp.391-403.

11. Hooper, J. D., and Irrgang, R. (1988) "Wall Shear Stress Measurement - A Comparison of the Directional Response of the Preston, Stanton, and Wall Block Probes," Experimental Heat Transfer, Fluid Mechanics, and Thermodynamics 1988, Eds. R. K. Shah et al., Elsevier, N. Y., pp. 1720-1725.

12. Haritonidis, J. H. (1989) "The Measurement of Wall Shear Stress," Advances in Fluid Mechanics Measurements, Lecture Notes in Engineering, Ed. M. Gad-el-Hak, Springer-Verlang, Berlin, pp. 229-261.

13. Fage, A., and Falkner, V. M. (1931) "On the Relation Between Heat Transfer and Surface Friction and Laminar Flow," Aero. Res. Counc. , R&M, No. 1408.

14. Ludweig, H., and Tillman, W. (1949) "Untersuchungen uber die Wandschubspannung in turbulenten Reibungschichten," Ing. Arch., Vol. 17 pp. 288-299. Investigations of the wall shearing stress in turbulent boundary layers, NACA TM 1285 (1950).

15. Liepmann, H. W. and Skinner, G. T. (1954) "Shear-Stress Measurements by Use of a Heated Element," NACA TN 3269.

16. Bellhouse, B. J., and Schultz, D. L. (1966) "Determination of Mean and Dynamic Skin Friction, Seperation, and Transition in Low-Speed Flow with a Thin-Film Heated Element," Journal of Fluid Mechanics, Vol. 24, pp. 379-400.

17. Bellhouse, B. J., and Schultz, D. L. (1968) "The Measurement of Fluctuating Skin Friction in Air with Heated Thin-Film Gauges," Journal of Fluid Mechanics, Vol. 32, part 4, pp. 675-680.

18. Diller, T. E., and Telionis, D. P. (1989) "Time-Resolved Heat Transfer and Skin Friction Measurements in Unsteady Flow," Advances in Fluid Mechanics Measurements, Lecture Notes in Engineering, Ed. M. Gad-el-Hak, Springer-Verlag, Berlin, pp. 323-355.

19. Lefebvre, P. J., and LaPointe, K. M. (1986) "The Effect of Mounting Position on Hot-Film Wall Shear Stress Sensors," AIAA Paper No. 86-1101.

20. Hanratty, T. J., and Campbell, J. A. (1983) "Measurement of Wall Shear Stress," Fluid Mechanics Measurements, Ed. R. J. Goldstein, Hemisphere Pub. Corp., N. Y., pp. 559-615.

21. Cole, K. D., and Beck, J. V. (1988) "Conjugate Heat Transfer from a Hot-Film Probe for Transient Air Flow," ASME Journal of Heat Transfer, Vol. 110, pp. 290-296.

22. Menendez, A. N., and Ramaprian, B. R. (1985) "The Use of Flush-Mounted Hot-Film Gauges to Measure Skin Friction in Unsteady Boundary Layers," Journal of Fluid Mechanics, Vol. 161, pp. 139-159.

23. Nandy, S., and Tarbell, J. M. (1986) "Flush-Mounted Hot Film Anemometer Accuracy in Pulsatile Flow," ASME Journal of Biomechanical Engineering, Vol. 108, pp. 228-231.

24. Cook, W. J., and Giddings, T. A. (1988) "Response of Hot-Element Wall Shear-Stress Gages in Laminar Oscillating Flows," AIAA Journal, Vol. 26, pp. 706-713.

25. Monson, D. J. (1984) "A Laser Interferometer for Measuring Skin Friction in Three-Dimensional Flows," AIAA Journal, Vol. 22, pp. 557-559.

26. Klein, E. J., and Margozzi, A. P. (1969) "Exploratory Investigation of the Measurement of Skin Friction by Means of Liquid Crystal," NASA TM X-1774.

27. Klein, E. J., and Margozzi, A. P. (1970) "Apparatus for the Calibration of Shear Sensitive Liquid Crystals," Review of Scientific Instrumentation, Vol. 41, pp. 238-239.

28. Schultz-Grunow, F. (1940) "Neues Reiungswiderstandsgesetz fur glatte Platten," Luftfahrtforschung, Vol. 17, pp.239-246, 1940. "New Frictional Law for Smooth Plates," NASA TM 986 (1941).

29. Dhawan, S. (1953) "Direct Measurements of Skin Friction," NACA Report 1121.

30. Allen, J. M. (1976) "Systematic Study of Error Sources in Supersonic Skin-Friction Balance Measurements," NASA TN D-8291.

31. Allen, J. M. (1980) "Improved Sensing Element for Skin-Friction Balance Measurements," AIAA Journal, Vol. 18, pp. 1342-1345.

32. Schmidt, M. A., Howe, R. T., Senturia, S. D., and Haritonidis, J. H. (1988) "Design and Calibration of a Microfabricated Floating-Element Shear-Stress Sensor," IEEE Transactions on Electron Devices, Vol. 135, pp. 373-380.

33. Nitsche, W., Mirow, P., and Szodruch, J. (1989) "Piezo-Electric Foils as a Means of Sensing Unsteady Surface Forces," Experiments in Fluids , Vol. 7, pp. 111-118.

34. Voisinet, R. P. (1979) "Combined Influence of Roughness and Mass Transfer on Turbulent Skin Friction at Mach 2.9," 17th Aerospace Sciences Meeting, 79-0003.

35. Roensch, R. L., and Cadwell, J. D., "Direct Measurement of Skin Friction in a High Reynolds Number Supersonic Blow-Down Wind Tunnel," Douglas Paper 1728, Douglas Aircraft Company.

36. Bruno, J. R., and Risher, D. B. (1968) "Balance for Measuring Skin Friction in the Presence of Ablation," NOLTR 68-163, U. S. Naval Ordinance Lab., White Oak, Md.

37. Orth, R. C., Billig, F. S., and Grenleski, S. E. (1974) "Measurement Techniques for Supersonic Combustion Testing," Progress in Astronautics and Aeronautics, Vol. 34, pp. 263-282.

38. DeTurris, D. J., Schetz, J. A., and Hellbaum, R. F. (1990) "Direct Measurements of Skin Friction in a Scramjet Combustor," AIAA Paper 90-2342.

39. Hager, J. M., Simmons, S., Smith, D., Onishiv S., Langley, L. W., and Diller, T. E. (1990) "Experimental Performance of a Heat Flux Microsensor," ASME Paper 90-GT-256. Also accepted for ASME Journal of Turbomachinery.

40. Putz, J. M. (1991) "Development of Instrumentation for the Support of Skin Friction Measurements," M. S. Thesis, Virginia Polytechnic Institute and State University, Blacksburg, VA.

41. Analog Devices Instrumentation & Isolation Amplifiers , Vol. 1, pp. 5:43-5:54.

42. Andraka, C. E., and Diller, T. E. (1985) "Heat Transfer Distribution Around a Cylinder in Pulsating Crossflow," ASME Journal of Engineering for Gas Turbines and Power, Vol. 107, pp. 976-982

43. Incropera, F. P., and DeWitt, D. P. (1985) Fundamentals of Heat and Mass Transfer, 2nd Ed., John Wiley & Sons, New York, p. 351.

44. Putz, J. M., Putz, J., Wicks, A. L., and Diller, T. E. (1990) "Thin-Film Shear Stress Gage," accepted for Symposium on Micro-Structures, Sensors, and Actuators of the ASME Winter Annual Meeting, Dallas, Texas.

Vita

The author was born on October 2, 1967, in the small town of Twinsburg, Ohio. He began his Bachelor of Science degree in Mechanical Engineering in August of 1985 at Virginia Polytechnic Institute and State University. After recieving his B. S. degree in May of 1989, he decided to continue his education by obtaining a Master of Science degree in Mechanical Engineering at VPI & SU. After completion of this thesis, the author plans to begin working for the HPI Corporation in Charleston, SC, in the development of a high pressure fuel injection system.

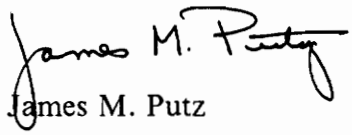

James M. Putz